LUND UNIVERSITY

Master Thesis

Development of a thiol-ene microfluidic Concanavalin A (ConA)-functionalized chip for retention of glycoproteins and subsequent CE-UV analysis

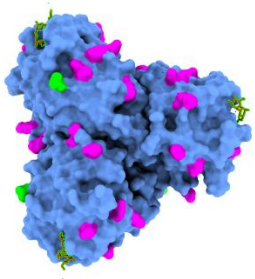

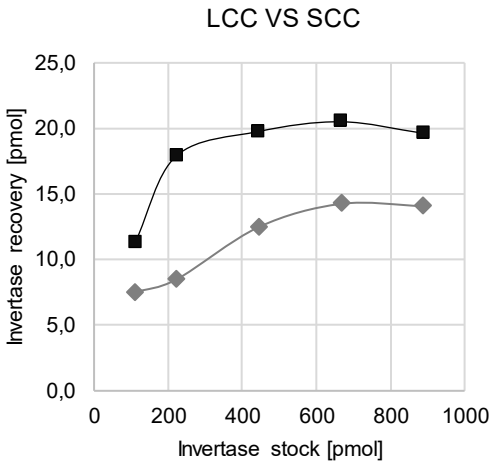

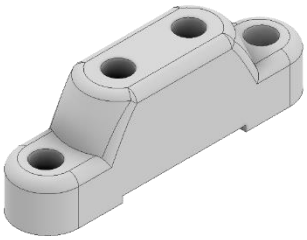

Monika Rosa Fürnsinn

Supervisors:

Jörg P. Kutter, Group Leader, Microscale Analytical Systems laboratory, Department of Pharmacy, Faculty of Health and Medical Sciences, University of Copenhagen

Johan Nilsson, Biomedical Engineering, LTH – Lund University

Examiner:

Rajni Hatti-Kaul, Biotechnology, LTH – Lund University

26.06.2025

Popular Science Abstract

Proteins often carry sugar molecules that play an essential role in how cells communicate, respond to their environment, and function properly. These “sugar-coated” proteins are called glycoproteins. The patterns of the sugar chains on the protein surface are unique. Changes in these sugar patterns can be early warning signs for many diseases, including cancer, making them a valuable target for medical research. However, studying glycoproteins is complex: traditional methods for separating and analyzing glycoproteins are slow, wasteful, and often loose some of the proteins along the way.

This thesis explores a new small microfluidic chip device that can capture glycoproteins using a sugar-binding protein called Concanavalin A (ConA). Inside the chip channel there is a sponge-like material (a monolith), which increases the surface area for capturing proteins. On this monolith the ConA is permanently fixed and binds the glycoproteins while they pass by. This small device helps capture the glycoproteins efficiently, using less time, fewer chemicals and smaller samples than traditional methods. Employing invertase, a glycoprotein, as a model protein, the system’s performance was tested under different conditions. For example, different designs of the chip channel were examined to see which worked best. The design featuring a longer channel was better at collecting the invertase but required very slow flow to avoid damaging the monolith inside the channel.

In conclusion, this work is a step forward towards fixing a lectin inside the monolithic channel in order to isolate glycoproteins on a small scale. While more development is needed to improve reliability, the device offers a foundation for future tools in biomedical research and diagnostics.

Abstract

The selective separation of glycoproteins is essential in biomarker discovery, glycoprotein profiling and analysis. Glycosylation of proteins has a major impact on their structure and function. The heterogeneity of glycosylation patterns makes the glycomic profiling extensive, but nonetheless of upmost importance for the deeper understanding of metabolic pathways, cell signalling and the impact of glycosylation alterations. The conventional methods for (glyco)protein analysis from biological samples, come with tedious sample preparation, that also have high reagent use and sometimes lead to loss of protein. By combining loading, washing and elution in one microfluidic device, loss of protein, sample preparation time and reagent waste can be minimized.

This thesis work aimed to develop a microfluidic lectin affinity platform for the selective separation of glycoproteins, utilizing a Concanavalin A (ConA)-functionalized "monolithic" chip. The immobilisation of a non-enzymatic protein on a thiol-ene monolith chip is, to our knowledge, a novel approach.

Using invertase as a model glycoprotein, the system is systematically characterized under varying sample concentrations, buffer and flow conditions to evaluate binding efficiency, elution performance and chip capacity. Despite the variability in yield between the chip replicates the system demonstrated the ability to bind invertase and recovering it via competitive elution with methyl-α-D-mannopyranoside. Two different channel designs were tested, and their performance and flow characteristics were compared to each other. The long channel chip (LCC) with a smaller cross section resulted in higher recovery yield than the short channel chip (SCC), however pressure drop calculations reveal that the operating flow rates for the LCC have to be around 2 µL/min to not disrupt the monolith structure in the channel. The maximum amount of invertase eluted off the LCC and SCC was measured with CE-UV to be ~20 pmol and ~15 pmol, respectively.

Overall, this work presents a promising step toward integrating lectin affinity chromatography into microfluidic systems for glycoprotein handling. The immobilization of ConA on a thiol-ene monolith and the demonstrated binding of a model glycoprotein mark an advance toward miniaturized, efficient sample preparation workflows. While further optimization of the system is required to enhance reproducibility and binding capacity, the platform lays the groundwork for future applications.

Key words: Lectin-functionalized microfluidic device; Thiol-ene monolith; Concanavalin A; Invertase; Methyl-α-D-mannopyranoside; Capillary electrophoresis; Design and flow optimisation.

Table of Contents

1. List of Abbreviations

3A	1,3,5-triallyl-1,3,5-triazine-2,4,6 (1H,3H,5H)-trione
4T	Pentaerythritol tetrakis (3-mercaptopropionate)
ASA	L-Ascorbic Acid
BGE	Background electrolyte
CE	Capillary electrophoresis
ConA	Concanavalin A
CRD	Carbohydrate-recognition domain
E	Elution fraction
EOF	Electroosmotic flow
HCl	Hydrochloric Acid
Inv	Invertase flow through fraction
K_A	Affinity constant
K_D	Dissociation constant
LAC	Lectin Affinity chromatography
LCC	Long channel chip
LPA	Linear polyacrylamide
MeOH	Methanol
MQ	Milli-Q
MαM	Methyl-α-D-mannopyranoside
OSTE	Off-stochiometric thiol-ene
PDMS	Polydimethylsiloxane
PEW	Pre-elution wash
PMMA	Poly-methylmethacrylate
SCC	Short channel chip
t-Boc	2–tert(butoxycarbonyl-amino)ethanethiol
TRIS	Tris(hydroxymethyl)aminomethane
UV	Ultraviolet
W	Wash fraction

2. Introduction

2.1 Starting point of this project

The fundament of this project was created by Aoife McLoughlin who established a working protocol for monosaccharide methyl-α-D-mannopyranoside (MαM) extraction from simple solutions (McLoughlin, A., n.d, 2025). Further, invertase was bound, eluted off and indirectly detected via an invertase assay, exploiting its catalytic ability for sucrose hydrolysis. The reaction products were detected via a capillary electrophoresis-UV (CE-UV) method for monosaccharide detection. Her project laid the groundwork and showed that on-chip carbohydrate binding with the immobilized Concanavalin A (ConA) was possible.

This project aimed to further develop the chip by focusing on glycoproteins, attempting to quantify the binding capacity of the system and testing different channel designs. Future perspectives included the optimization of the flow protocol and time efficiency. The CE-UV protocol was optimized for proteins and the runtime for one sample was set down to 15-20 min (5 min replenishment step, 5 min wash step, 5-10 min separation).

In Figure 1 the schematic illustration of the idea behind the protocol is illustrated. The sample matrix with glycoproteins and ions or other molecules is loaded on the chip. The glycoprotein binds to the lectin and the non-bound glycoproteins gets washed off together with the sample matrix. Competitive elution released the bound glycoproteins which further are analysed by CE-UV detection.

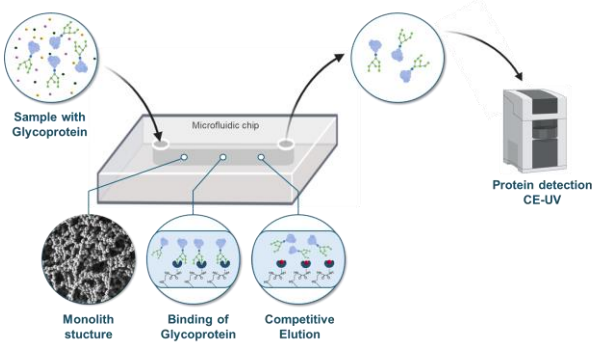

Figure 1: Schematic illustration of the chip design and the lectin-glycoprotein interaction. The channel is filled with a monolith, a porous high surface structure, which was chemically pretreated to allow lectin immobilization. The glycoproteins are bound by the lectin, non-bound are washed off and bound glycoproteins are subsequently eluted off by competitive elution with monovalent sugar (Scientific Image And Illustration Software | BioRender, o. D.).

2.2 Glycoproteins

Glycoproteins are very important in numerous biological processes in various organisms. The covalent attachment of sugar residues to the surface of the protein structure plays a major role in the functional specialization of proteins and influences processes like cell signalling, recognition, cell adhesion and catalysis (He et al., 2024). The glycosylation of proteins can vary a lot and is very characteristic for the function of the protein or peptide. Furthermore, it is one of the most abundant post-translational

modification of proteins and for example appears in up to half of the proteins in human plasma (Yang & Hancock, 2004).

Abnormal alterations in glycosylation patterns are widely recognized as biomarkers for various pathological conditions (Reis et al., 2010), (He et al., 2024). For example, in various rheumatic and respiratory disorders the glycosylation pattern of proteins in immune response is modified, due to a change in glycosylation pathways (Kissel et al., 2022), (Xu et al., 2024b). Tumour progression and transformation is influenced by glycosylation alterations among other post-translational modifications (Bangarh et al., 2023). One example is the epidermal growth factor receptor 2 (HER2), a glycoprotein and an important tumour progression marker (Silsirivanit, 2019).

However, the structural complexity and heterogeneity of glycoproteins, combined with their often low abundance in biological samples, present major analytical challenges (Mariño et al., 2010). Selective enrichment and purification are therefore essential steps for accurate glycoprotein analysis, profiling and biomarker discovery.

2.3 Analytical methods for glycoprotein analysis

Modern protein analysis techniques, like mass spectrometry, require careful sample handling. Complex sample matrices result in uninterpretable signals, thus the proteins of interest have to be extracted, purified and resuspended in method-compatible buffers. Most proteins are suspended in buffers with different additives to ensure stability. However, the buffer ions and other additives can interfere with analytical signals, mostly resulting in lower sensitivity of the analytical method (Ocaña-González et al., 2015). Hence, there is a need for sample preparation techniques that allow a choice in resuspension buffer or matrix, so a variety of analytical methods and injection modes can be used subsequently.

One major limitation of traditional sample preparation methods is that they are labour-intensive, require a large amount of sample and reagents and can lead to the loss of the proteins of interest. The current gold standard method for glycomic profiling is mass spectrometry, which requires multiple sample preparation steps (Bosques et al., 2006). Microfluidic systems can address this challenge by using only a sample fraction and allow analysis with low power consumption, low reagent use and high sensitivity. Further, they can improve the speed of analysis by promoting reaction kinetics through small diffusion distances (Pagaduan et al., 2015). The development of microfluidic platforms for biomarker extraction and detection is on the rise. There is still the need for a combination of methods, like lectin functionalized matrix or selective extraction and an analytical method for rapid identification of protein glycosylation-patterns (Mariño et al., 2010), (Pagaduan et al., 2015).

To tackle these challenges, we have started to develop a microfluidic chip specifically designed for the selective extraction of glycoproteins using lectin affinity capture. The chip incorporates a ConA-functionalised monolith that binds glycoproteins, that contain hybrid-type N-glycans (Lis & Sharon, 1998). By integrating binding, washing, and elution into a single microfluidic platform, this system aims to minimize sample handling, reduce protein loss, and enhance enrichment efficiency.

2.4 Lectin Affinity Chromatography

Lectin affinity chromatography (LAC) has shown to be an excellent tool for extracting polysaccharides, glycoproteins or glycopeptides from various samples (O'Connor et al., 2016). One of the most recent advances in glycoprotein purification with LAC is described by Da Silva et al. (2024), where the Rabies virus recognition glycoprotein was purified and subsequently analysed and tested for activity.

Proteins that reversibly and selectively bind sugars are called Lectins. They are able to bind a broad range of glycans, from simple sugars to oglio- and polysaccharides. The biological function of lectins is the recognition of carbohydrates on cell surfaces, within cells and in physiological fluids (Ashwell & Morell, 1977), (Sharon, 2004).

Lectins are found in different organisms ranging from microorganisms, like bacteria and amoeba, over animals and to plants and serve diverse roles. In animals they are mostly associated to immune response (e.g. macrophage mannose receptor in the innate immune response), cell-cell interactions between cells in immune and neural system (e.g. siglecs) or cell-adhesion (e.g. spermadhesin) (Sharon, 2004), (Töpfer-Petersen et al., 2009). They can also be found in plant seeds and vegetative organs and are capable of agglutination (Goldstein et al., 1965). In plants their role is not fully understood nor proved, but it is argued that they could serve as protection against phytopathogenic fungi and are insecticidal (Barkai-Golan et al., 1978), (Janzen et al., 1977), (Van Damme, 2021).

Lectins possess a short unique amino acid sequence, that is able to recognise sugars and polysaccharides and is called carbohydrate-recognition domain (CRD). It has a characteristic fold and is in close proximity to the carbohydrate-binding region. The CRD alone does not account for the specificity of a lectin as same sugar can be recognized by multiple CRDs (Surya et al., 2020).

Most lectins bind the terminal end of a glycan chain, however there are others that recognize and bind sugars within the chain. Lectins bind carbohydrates over non-covalent weak bonds, including Van-der-Waals interactions (Coelho et al., 2017), hydrogen bonding and hydrophobic interactions (Sharon, 2004b).

2.4.1 Multivalency and Cluster Glycoside Effect

Lectin-sugar binding methods are similar to immunoaffinity techniques but differ greatly in the protein that is used for capturing and association/disassociation constants. It has been reported that lectin-glycan interactions have a lower affinity constant of $10^4 \leq K_A \leq 10^7$ M^{-1} than antibody-antigen binding with $10^8 \leq K_A \leq 10^{12}$ M^{-1} (Kuno et al., 2005), (Tousi et al., 2010), (Shang et al., 2016). To reach binding equilibrium, longer incubation times, closer control of flow rates and lectin density needs to be applied (Shang et al., 2016).

However, the cluster glycoside effect can affect the carbohydrate-lectin affinity (Smith et al., 2003), (Lee & Lee, 2000). This high affinity between polyvalent carbohydrate ligands (glycosylated proteins)

and polyvalent lectins is caused by the multiple simultaneous attachment events, which affect the overall strength of interaction and help overcome the free energy of single interactions (Müller et al., 2016).
Most lectins are multivalent, meaning that they have multiple binding sites. Glycoproteins with extended sugar structures can make additional contacts with the lectin, which increases the avidity. The affinity can also be increased by the bridging of multiple lectins (that are in close proximity to each other) by the several carbohydrate units on a single glycoprotein. When bound to multiple binding sites on one lectin or bridging, slower dissociation occurs because the breaking of all interactions is entropically unfavoured (Dam et al., 2000).
The multivalent binding by the lectin is a non-cooperative event, meaning that the lectin-binding sites are independent from each other (Reynolds & Perez, 2011). However, after first attachment to one binding site of a lectin, the other clustered ligand carbohydrate residues are in close proximity to other intra-molecular binding sides. The increased local concentration near the lectin surface most likely leads to the next binding occurrence (Müller et al., 2016).

2.4.2 Concanavalin A

The focus of this work is the lectin ConA, which is isolated from the jack bean seed (*Canavalia ensiformis*). As can be seen in Figure 2 ConA is a homotetrameric protein at physiological pH. ConA is not catalytically active, but it is able to bind α-D-mannose and α-D-glucose residues. These two hexoses are similar in structure except for the orientation of the alcohol group on carbon in position 2. ConA is able to bind more complex structures, for example N-glycans or hybrid-antennary glycan complexes. It interacts with these through binding α-D-mannosyl and α-D-glucosyl residues in terminal position (Lis & Sharon, 1998).

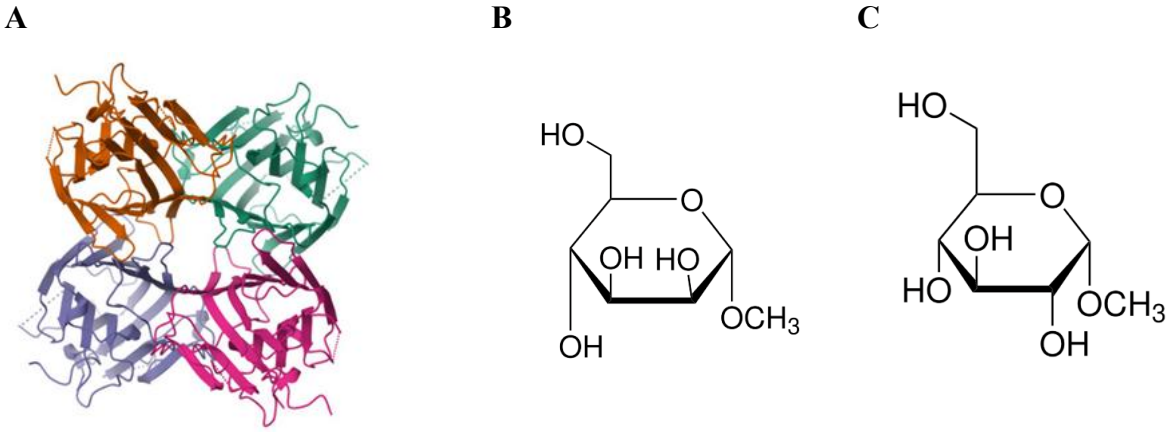

Figure 2: (A): Homotetrameric stucture of ConA with a molecular weight of 106 kDa (Bouckaert et al., 1995b).
(B): Methyl-α-D-mannopyranoside (Methyl A- D -mannopyranoside = 99.0 HPLC 617-04-9, o. D.)
(C): Methyl α-D-glucopyranoside (Methyl A- D -glucopyranoside = 99 97-30-3, o. D.)

As described in the review of Saleemuddin and Husain (1991), due to its carbohydrate binding properties and its relatively cheap commercial price, ConA has been used in various chromatography applications and enzyme-bed-reactors and has been immobilized on matrixes like Sephadex, Agarose and magnetic beads (Fujiwara et al., 2021).

For instance, the publication of Selzer et al. (2022b) describes how ConA was immobilised via carboxylate residues on magnetic beads for the subsequent immobilisation of glucose oxidase. They further investigated the alteration of the binding between ConA and Glucose oxidase in the presence of bovine serum albumin. Another example would be Goumenou et al. (2024), where the application of a Sepharose-ConA surface plasmon resonance application was developed. This was used for the characterisation of various hCG glyco-isoforms (Dixit, 2022).

When developing a system that incorporates immobilised proteins, it is important to consider the structural features and essential environment that are necessary to preserve the activity the proteins. The stabilization of the active carbohydrate binding conformation of ConA is reliant on the presence of the divalent metal ions manganese and calcium near the carbohydrate-binding site (Sumner & Howell, 1936), (Kalb & Levitzki, 1968), (Shoham et al., 1973), (Brewer et al., 1983). Removal of these ions, especially Ca^{2+}, leads to major conformational shifts, including the disruption of the Ca^{2+} binding site and a cis-to-trans isomerization of the Ala207-Asp208 peptide bond, which is normally stabilized by Ca^{2+}. These changes alter the loop containing the binding residues (Leu99, Tyr100) and displace others (Asn14, Arg228, Asp208), effectively eliminating sugar-binding capability (Bouckaert et al., 1995).

The pH stability of soluble ConA is reported to be between pH 2 and 9.8 (Nonis et al., 2021). The interaction with the monovalent sugar α-methyl-D-mannoside is shown to occur over a wide pH-range of pH 4 to 8 (Pflumm et al., 1971), (Hassing & Goldstein, 1970). While the overall tetrameric structure is retained at pH 5, loss of metal coordination weakens inter-dimer interactions. This could explain ConA's pH-dependent dissociation below pH 6.5 into two dimers (Bouckaert et al., 1995).

The long-term thermal instability of ConA under physiological conditions (room temperature, 0.15 M NaCl, ~ pH 7.5) can be a limiting factor in lifetime and efficacy of ConA in various assays (Locke et al., 2014). Throughout this work, this limitation was tackled by keeping the chips on ice during experimental procedures and stored at 4°C.

2.5 Thiol-ene Click chemistry

ConA is immobilised inside the microfluidic channel on a porous monolith. In chromatographic terms a monolith is a single (greek 'mono') column (or stone, greek 'lithos') of porous material (Hefnawy et al., 2023), (Tanaka et al., 2002). Thiol-ene click chemistry is used for the microfluidic chip fabrication and the functionalised in-channel monolith structure for the ConA immobilisation.

2.5.1 Stochiometric and off-stochiometric thiol-ene click chemistry

The monolith is formed using a light-induced thiol-ene click reaction between tetra-thiol monomers and tri-allyl monomers (see Figure 3). The crosslinking of these multifunctional groups is initiated by the addition of photoinitator and exposure to UV light and they create a thiol-ene net. By exposing the reaction mixture to UV light, the TPO-L photoinitiator is cleaved to a radical that abstracts the hydrogen atom from the thiol group of the tetra-thiol monomer. The now radicalised cleaved thiol group forms a

bond with an ene moiety of the tri-allyl monomer. This bond is formed with the carbon atom with the least substituents and creates a carbon-centred radical. When one carbon-centred radical meets another, they can form a covalent bound and are thus not able to be radicalised further. A stop to the polymerisation can be done by ending the exposure to UV light (Hillmering et al., 2016) (Lafleur et al., 2015b).

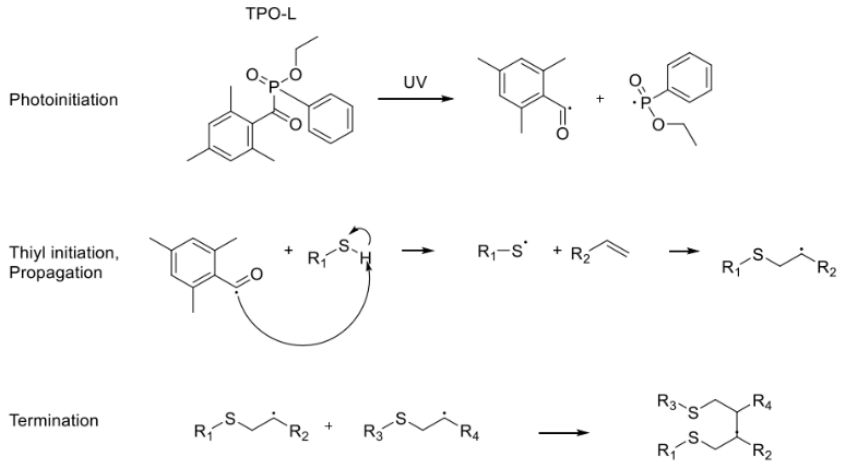

Figure 3: Schematic illustration of thiol-ene click chemistry with TPO-L photo initiator. Reproduced from Sønderby, C. (2018).

For creating the microfluidic chips, a stochiometric ratio of tetra-thiol monomers and tri-allyl monomers was used, creating a tight network without free unreacted groups at the surface. The mixture of the monomers was poured into a polydimethylsiloxane (PDMS) mold and cured under UV light. Although the polymerisation mechanism without the addition of a photo initiator is not fully understood, it can be assumed that the bond of the thiol groups is directly cleaved, leaving a reactive radical for propagating of the polymerisation (Lafleur et al., 2015b).

The off-stochiometric thiol-ene (OSTE) bead-like monolith was created inside the microfluidic channel, by an emulsion of both monomers, methanol and the photoinitiator. By adding one monomer in excess, the surface of the monolith structure can be manipulated. As can be seen in Figure 4, the off-stochiometric mix of the two monomers results in an excess of the monomers with the higher abundance. Methanol is not able to copolymerize and if added in a high amount of over 75%, it acts as a porogen that causes the monomers to form beads through polymerisation. As extensively described in Lafleur et al. (2015) the monolith bead size, density and uniformity greatly depend on the preparation conditions. The speed of stirring has one of the biggest impacts on the bead size. For chromatographic application a large bead surface area to volume ratio and uniform bead structure is desirable (Lafleur et al., 2015b).

1 **2**

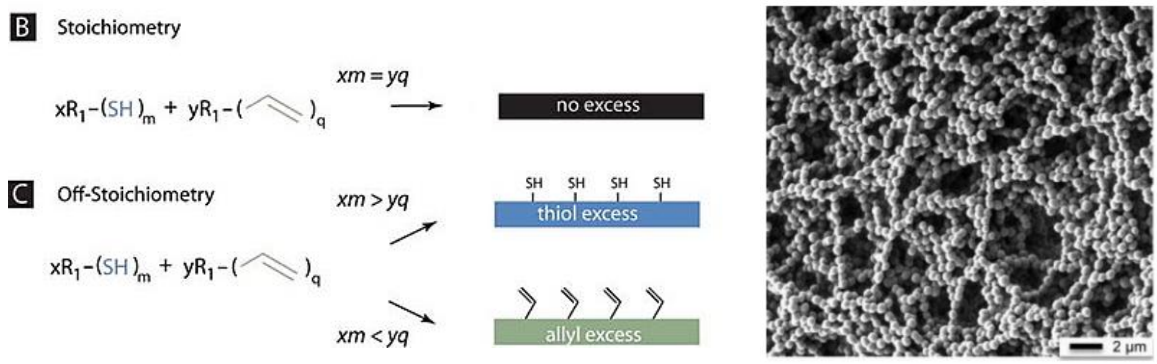

Figure 4: (1): B… Stoichiometric mixture of monomers result in complete polymerisation and inert surface. C…Off-stoichiometry mixture of monomers causes excess off unreacted thiol (xm>yq) or ene groups (xm<yq) on the surface (Carlborg et al., 2011).
(2): SEM picture of bead-like thiol-ene monolith with porogen (>75% methanol) (Lafleur et al., 2015b).

2.5.2 Immobilization on OSTE-allyl monoliths via click chemistry and ASA linkage

ConA was covalently immobilised on the bead-like OSTE monolith with 40% excess of ene-functional groups on the surface (see Figure 5). The 2–tert(butoxycarbonyl-amino)ethanethiol (*t*-Boc)-protected cysteamine linker, contains both a primary amine and a thiol group. The thiol group reacts with the surface ene-funcitonal groups via photochemical radical-mediated thiol-ene addition (exposure to UV light and presence of 5% TPO-L in ethanol). This results in a stable thioether bond and a protected amine at the terminus. The Boc-protection group is eliminated by exposure to acidic conditions, resulting in a free primary amine, that is able to react with the L-ascorbic acid (ASA; 1% w/v in MeOH). The ASA can act as a di-keto coupling agent and links the free amino group and the free primary group of lysing and N-terminus of ConA (Lafleur et al., 2015). In Figure 6 all lysine residues and the N-terminus are marked in the overall structure of the ConA homotetramer, complexed with trimannosides. As can be seen, there is no lysine residue in the binding site, suggesting that this immobilisation method does not disrupt a binding site by the covalent bound. However, the immobilisation is not orientated and thus it cannot confidently be stated that all binding sites are sterically available.

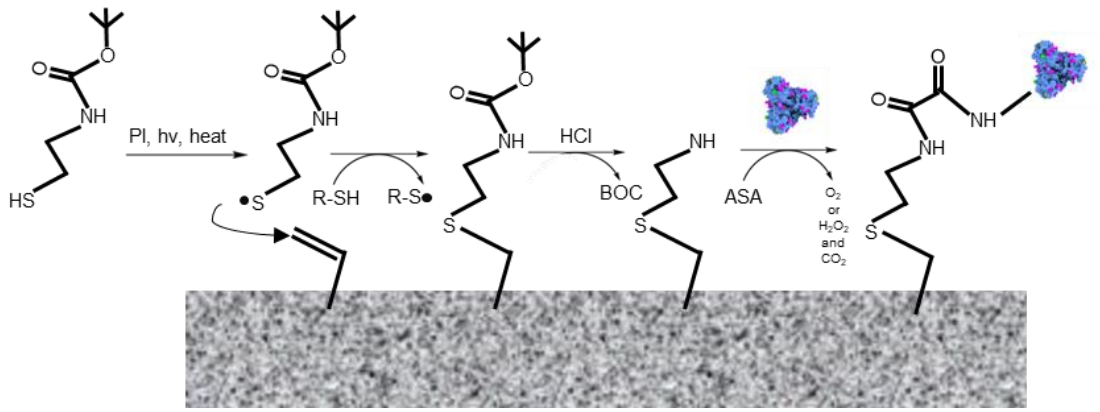

Figure 5: Covalent immobilization of Concanavalin A (ConA) onto a thiol-ene monolith. Reproduced from unpublished schematic illustration in the Microscale Analytics group, KU. (Protein structure from PDB, Naismith & Field, 1996).

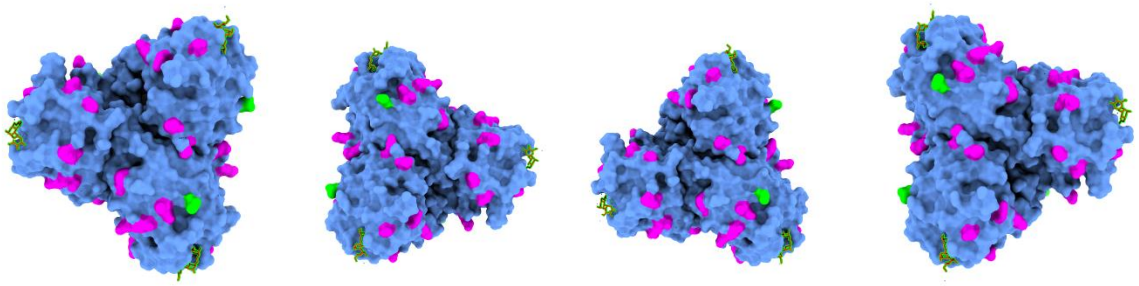

Figure 6: 360° view of ConA structure complexed with trimannoside. Purple: Lysine residues on the protein surface. Green: N-Terminus of the subunits. Green-Red: Trisaccharide in binding pocket. Pictures were generated in ChimeraX. (Protein structure from PDB, Naismith & Field, 1996).

2.6 Invertase as a Model Glycoprotein

For testing the ConA-functionalised chip, this work utilized invertase, a highly glycosylated enzyme that catalyses the sucrose hydrolysis into the monosaccharides glucose and fructose. Invertase is a beta-fructofuranosidase (EC.3.2.1.26) and can be isolated from *Saccharomyces cerevisae* (Sainz-Polo et al., 2013). In this thesis work invertase is used as a 'model glycoprotein'. Since yeast can produce glycosylation patterns similar to mammalian cells, external invertase can be used as a model for the study of lectin-affinity (Hamilton & Gerngross, 2007).

Invertase from yeast occurs in two forms: internal and external invertase. Internal invertase is non-glycosylated, while external invertase contains 50% mannan and 2-3% glucosamine in its glycan structures, making it very suitable for the binding to ConA. It exits as a dimer, but it can also associate into tetra-, hexa- and octameric structures. The formation of these multimers and the association-dissociation equilibrium position very much depends on the glycosylation extent, because the carbohydrate chains have a stabilizing function (Chu et al., 1983).

External invertase has 14 possible N-glycosylation sites, resulting in a highly glycosylated protein structure (Zeng, et al., 1999). It has been reported that nine of these sites contain short oligosaccharide chains with a core structure of two N-acetylglucosamine ($GlcNAc_2$) and outer branches with 8 to 14 mannose units. Of the remaining sites, four contain wide range of different lengths of oligosaccharide chains. These also contain a $GlcNAc_2$ core and a mannose content of over 50 units. One site appears to be without glycosylation. (Reddy et al., 1988), (Zeng, et al., 1999).

As has been reported by the former student Aoife McLoughlin, the eluted invertase showed activity in an invertase assay. This highlights the potential of this chip for mild sample preparation. In the assay, invertase was mixed with sucrose and the ratio of glucose and fructose was measured via CE-UV. For protocol and result details see Appendix A.

2.7 Capillary Electrophoresis with UV detection

For the detection of the glycoprotein amount in the different fractions of the microfluidic system a method for CE of the intact proteins was employed. This method was chosen due to its compatibility

with microfluidic systems, because of low sample amounts. At the start of this project the idea was to separate glycoprotein from non-glycoprotein on the chip and detect both in the sample. However, due to time restraints and the high chip-to-chip variability this was not possible to be investigated.

The main advantage of CE is the separation of analytes based on their charge-to-size ratio and the low sample consumption, which makes it ideal for the combination with microfluidic applications (Andrasi et al., 2023b). Further, it can be connected to mass spectrometry and UV detection. The analyte is injected into the background electrolyte (BGE) filled fused silica capillary and an electric field is applied. The applied voltage causes the BGE ions to form a fixed and diffuse layer close to the capillary wall. It also causes the diffuse layer to migrate towards the electrode of opposite charge. This electroosmotic flow (EOF) (μ_0) is the bulk flow of the ions in the diffuse layer and depends on the ionic strength of the BGE (ε), the charge of the capillary wall (zeta potential, ζ) and the viscosity of the BGE (η) (Schmitt-Kopplin & Fekete, 2016).

$$\mu_0 = \frac{\varepsilon\zeta}{\eta}$$

Also, the injected charged molecules migrate based on their electrophoretic mobility (μ_e) which is determined by their hydrodynamic size (r), their net charge (q) and the viscosity of the BGE (η). The net charge is again dependent on the pI of the protein and the sample matrix (Schmitt-Kopplin & Fekete, 2016).

$$\mu_e = \frac{q}{6\pi\eta r}$$

The observed mobility of the analytes is the sum of the EOF and the electrophoretic mobility and is called the effective mobility (μ_a) (Altria, 2003).

$$\mu_a = \mu_e + \mu_0$$

Depending on the ionic strength of the BGE, the length of the capillary, the separation conditions and injection mode this technique offers finetuning of separation.

2.7.1 Linear Polyacrylamide coated capillaries

The permanent coating of the inner surface of the capillary with a polyacrylamide layer masks the negative silanol-surface charges, creating a neutral hydrophilic surface. This effectively reduces protein-wall interactions, leading to less peak tailing and improves reproducibility (Andrasi et al., 2023b). Linear polyacrylamide (LPA) coated capillaries are very common for CE protein separation. Due to its covalent attachment, surface regeneration is not needed and thus opens possibilities for detection methods like MS (Hajba & Guttman, 2017). LPA coated capillaries are reported to demonstrate long term stability and give consecutive results over 100 runs (Andrasi et al., 2023b). The coating procedure can be divided into three steps, surface activation (etching), silanization and polymerization. The etching process opens the Si-O-Si bonds to make the Si-OH-group available for silanization (Hajba & Guttman, 2017). Between these steps the capillary inner surface must be dried thoroughly to allow efficient formation of

the intermediate and linear polymer layer (Cobb et al., 1990), (Courtois et al., 2006), (Andrasi et al., 2023b).

In LPA-coated capillaries the zeta potential $\zeta \sim 0$, and consequently $\mu_0 \sim 0$, $\mu_0 \sim \mu_a$, which leads to a separation based mostly on electrophoretic mobility of the proteins (μ_e). The separation of proteins in a LPA coated capillary with a BGE at a pH value lower than the pI, causes the injected proteins to carry a positive charge (Hamidli et al., 2021b), (Tran & Taverna, 2016).

2.7.2 Electrokinetic injection

Samples can be injected into the capillary via voltage that is applied to draw charged analytes into one end of the capillary. This leads to an enrichment effect of charged species at the injection interface. This injection bias for analytes with higher electrophoretic mobility has to be treated carefully. For reproducibility of measurements, sample matrix control is essential, because of the strong effect of the matrix ionic strength. The number of moles injected (n) depends on the concentration of the analyte in the sample (C), its electrophoretic mobility (μ_e), the electric field strength (E), the injection time (t_{inj}) and the cross-sectional area of the capillary (A) (Altria, 2003).

$$n = C * \mu_e * E * t_{inj} * A$$

3. Materials and Methods

Unless noted otherwise, all reagents were supplied by Sigma-Aldrich (Brøndby, Denmark). The chip and in-sito monolith production protocol are comparable to Lafleur et al. (2015) and Jönsson et al. (2017).

3.1 Microfluidic Chip Design and Fabrication

The initial short channel chip design (SCC), used prior to this thesis, featured a 12 mm-long, 500 µm-wide, and 300 µm-deep rectangular straight channel, with an internal channel volume of 1.5 µL. A second chip design was tested, featuring a longer channel chip (LCC) with a channel length of 73 mm with the same width, but 175 µm depth and a channel volume of 6.39 µL. The chips were operated using a syringe pump, with defined flow rates between 2 and 10 µL/min. The hydrodynamic resistance of the open (non-monolithic) channel was estimated using standard laminar flow theory for rectangular channels. The poly-methylmethacrylate (PMMA) master designs for both chips were already present in the lab. They were produced by designing the channels in the Autodesk software (Autodesk Inventor Professional 2015, San Rafael, CA; USA) and subsequently imprinting them onto PMMA plates with the high precision milling instrument (Minitech 3, Minitech Maschienery Cooperation, GA, USA).

3.2 PDMS Mold Preparation

The PDMS mold was prepared using a 10:1 ratio of Sylgard 184 silicone elastomer and its corresponding curing agent (Dow Chemical Company, Midland, MI, USA). The mix was degassed and filled onto the

PMMA master molds, which were then cured in an oven at 60°C overnight or 80°C for 2 hours. Finally, the PDMS molds underwent a 60 s Dymax curing step (Dymax EC 5000 Series UV curing flood lamp, Dymax cooperation, CT, USA).

3.3 Assembly of Chip and 3D-printed Holder

Pentaerythritol tetrakis (3-mercaptopropionate) (4T) and 1,3,5-triallyl-1,3,5-triazine-2,4,6 (1H,3H,5H)-trione (3A) were mixed in a stoichiometric ratio of 595.2 mg of 4T and 404.8 mg of 3A per g of chip material, followed by centrifugation at 3000 rpm for 5 min. The thiol-ene mixture was poured into the PDMS molds on a Teflon plate. The filled molds were sealed with lids and cured in the Dymax for 20 s per side (365 nm, 160 $mWcm^{-2}$). The cured chips were taken out of the PDMS molds, and the two halves were assembled. To minimize air entrapment, they were pressed together with a roller. The assembled chips were further cured for 60 s and placed under a weight for final stabilization. The chips were subjected to an additional 10 s UV cure shortly before further use.

The chip was placed in a chipholder that was modelled in the Autodesk software and printed with the Ultimaker 2 3D-printer (Geldermalsen, The Netherlands). For the connection between chip and Teflon tubing (Aarhus Mikrolab, Denmark), O-rings were placed between the chip and the chip holder to ensure sealing. A schematic illustration of the chipholder, the Autodesk mid-plane design, a photo of the chip holder and photos of SCC and LCC can be seen in Figure 7 A-E.

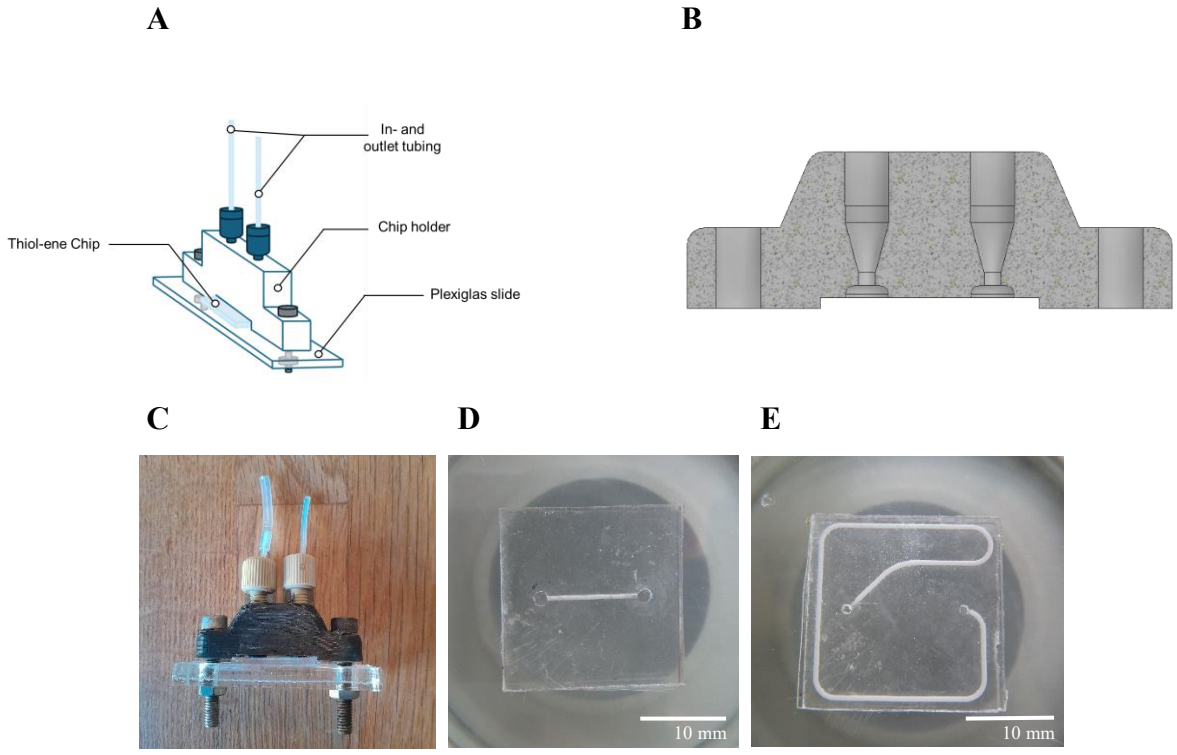

Figure 7: (A): Schematic illustration of the chip holder setup including inlet and outlet tubing. Dimensions are for illustrative purposes only and do not reflect the actual scale.
(B): Autodesk Chip holder design. Mid-plane.
(C): Photo of chip holder.
(D): Photo of SCC. E: Photo of LCC

3.4 Porous Monolith Synthesis

The production of the thiol-ene monolith was conducted in the dark room. The emulsion was prepared by mixing 4T and 3A in a 3:5.6 ratio (40% excess of 3A). A working solution was made by combining 375 mg of this mixture with 1.5 g methanol (MeOH) and 15 µL of the photoinitator TPO-L (10% v/v TPO-L in ethanol) (Luricin, BASF, Ludwigshafen, Germany), stirred at 400 rpm under light-protected conditions. To fabricate the monolith, 40–50 µL of the emulsion was pipetted into the SCC channel or 100 µL into the LCC channel and directly cured with the collimated UV lamp for 11 s (365 nm, LS-100-3C2, Bachur & Associates, CA, USA). The chip was flushed with MeOH at 5 µL/min for 20 min. After flushing, the monolith-filled chip was again cured for 11 s on both sides and was flushed with MeOH for 5 min. Functional chips were stored in methanol at 4°C until further use.

3.5 ConA Immobilisation

In order to immobilise the lectin ConA onto the chip, the allyl-excess surface of the monolith had to be functionalised with an amino group. In a light-protecting vial 10% TPO-L and *t*-Boc were mixed in a 1:20 w/w ratio. To the total amount of the TPO-L and *t*-Boc mixture, methanol was added in a 1:1 w/w ratio. This mixture was flushed through the chip at 5 µL/min for 5 min and cured on only one side for 60 s. Finally, the chip was flushed with methanol at 5 µL/min for 10 min. If not deprotected right away, the chip was stored in methanol at 4 °C.

The chip underwent a deprotection step, by flushing the chip with 4 M HCl at 2 µL/min for four hours (or 4 µL/min overnight) to remove the Boc-protecting groups and make the NH_2 groups available for the attachment of the ASA crosslinker. The ASA solution was prepared by dissolving 100 mg of ASA in a 1:2 (v/v) mixture of Milli-Q (MQ) water and MeOH, resulting in a total volume of 1.5 mL (7% w/v ASA in 66% MeOH). After washing the chip with MQ water with 10 µL/min for 10 min, the ASA solution was flushed through the chip at 10 µL/min for 10 min and then incubated at 1 µL/min for 30 min. After another wash, the chip was put on ice and 10 mg/mL ConA in 20 mM TRIS, 0.5 M NaCl, 1 mM $MnCl_2$, 1 mM $CaCl_2$, 2% Glucose, pH 7.5 was flushed through the chip at 2 µL/min for 30 min (total of 600 µg of ConA). Then the chip tubes were closed with parafilm, and it was stored at 4 °C overnight.

3.6 Experimental Workflow

A schematic illustration of the experimental workflow can be seen in Figure 8.

3.6.1 Invertase loading

The microfluidic chip was first equilibrated by flushing with 20 mM TRIS, 0.5 M NaCl, 1 mM $MnCl_2$, 1 mM $CaCl_2$ pH 7.5 for approximately 20 min to remove any residual glucose. Following equilibration, the invertase (from *Saccharomyces cerevisiae*, Sigma-aldrich, Cat. No. I4504) solution, dissolved in 20

mM TRIS, 0.5 M NaCl, 1 mM $MnCl_2$, 1 mM $CaCl_2$, pH 7.5 was introduced into the chip. A total of 60 µL was flushed through with 2 µL/min for 30 min and incubated for 30 min.

3.6.2 Pre-Elution Washing (PEW) Step

Unbound enzyme was removed by flushing the chip with running buffer for 10 min at 15 µL/min. Fractions were taken at the beginning of the PEW, each at 1 min (PEW1, PEW2, PEW3).

3.6.3 Competitive Elution with MαM

The outlet tubing was replaced, and the competitive elution of bound invertase was performed using MαM at a flow rate of 2 µL/min. Fractions were collected every 7.5 min for a total of three fractions (E1, E2, E3). The chip was subsequently neutralized with running buffer for 30 min at 10 µL/min, and an additional three fractions were collected at the end of the washing step by increasing the flow rate to 10 µL/min for 1.5 minute per fraction (W1, W2, W3).

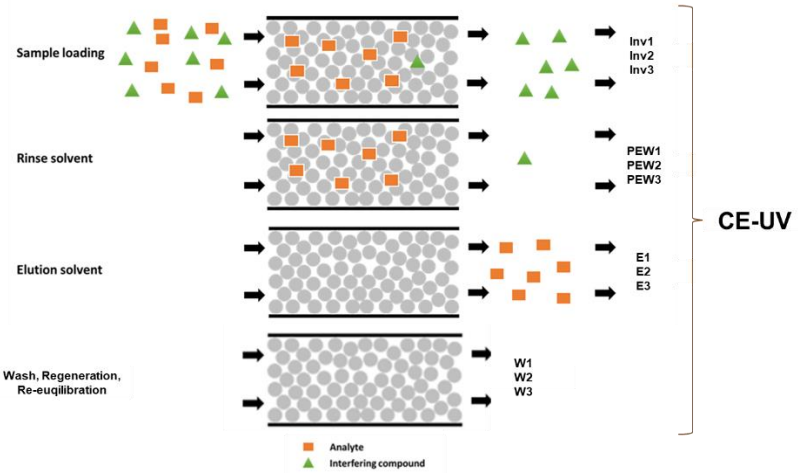

Figure 8: Schematic illustration of experimental workflow.

3.6.4 Chip Regeneration and Storage

The chip surface was regenerated by flushing the chip with 20 mM TRIS, 0.5 M NaCl, 1 mM $MnCl_2$, 1 mM $CaCl_2$ pH 8.5 at 10 µL/min for 10 min and flushing with 20 mM TRIS, 0.5 M NaCl, 1 mM $MnCl_2$, 1 mM $CaCl_2$, 2% Glucose pH 7.5. The chip was sealed and stored at 4°C until the next day.

3.7 Capillary Coating for CE

The coating of the bare-fused silica capillary was done according to Andrasi et al. (2023) and Hamidli et al. (2021). The pretreatment and coating of the capillary was done fully in the CE Instrument (7100 CE System, Agilent, Germany; coupled to a UV detector). Chemstation software (Agilent) was used for operating the CE instrument. The bare-fuse silica capillaries were purchased from Polymicro Technologies and had an inner diameter of 50 µm, outer diameter of 357 µm and a length of 65 cm (effective length to window 56.5 cm). After the coating procedure the capillary was cut down to 30 cm

(effective length to window 21.5 cm) from the inlet side. This was done to remove any inconsistently coated ends and to reach faster separation times.

The cassette temperature was set to 60°C for the whole process. The capillary was flushed with Acetone for 1 min at 6 bar (external pressure), 1 M NaOH for 10 min at 6 bar, MQ water for 1 min at 6 bar, 1 M HCl for 10 min at 6 bar and MQ water for 1 min at 6 bar. Then the capillary was dried with N_2 for 30 min at 6 bar. Next, 50% 3-(trimethoxysilyl) propyl methacrylate in methanol was flushed through the capillary at 6 bar for 5 min and incubated with both capillary ends in the reagent vials for 60 min. After the incubation, Acetone was flushed through for 2 min at 2 bar and following the capillary was N_2-dried again for 30 min at 6 bar. Two vials with each 1 mL of 4% Acrylamide were prepared and 10 µL of 10% Ammonium persulfate was added. Both were degassed with nitrogen for 5 min shortly before the vials were put in the CE autosampler. The capillary was flushed with the degassed acrylamide–ammonium persulfate mix for 5 min at 6 bar and incubated for 15 min by leaving each capillary end into the reagent vial. Then the capillary was taken out of the CE instrument and flushed with a syringe pump containing MQ water for 100 µL/h until a gel-like substance came out of the capillary. Afterwards, the capillary was cut down to 30 cm and put back into the CE instrument, where it was flushed with 100 column volumes with MQ water.

3.8 CE-UV Sample Analysis

The coated capillary was preconditioned by washing with BGE 50 mM Formic Acid for 5 min at internal pressure. The sample was injected via electrokinetic injection at 20 kV for 20 s at the cathodic end. The sample matrix was at neutral pH and the BGE at pH 2.6. Under these conditions, the invertase, having a pI around 4 (Product sheet, Invertase from *Saccharomyces cerevisiae*, Sigma-aldrich n.d,), is negatively charged in the sample solution and thus migrates electrophoretically toward the anode (positive charge), consequently the negatively charged protein is driven into the capillary. Due to the low pH of the BGE, the protein becomes protonated and decelerate, which leads to a focus at the interface. This pH-mediated stacking effect improves concentration sensitivity. For separation, the charges of the electrodes were reversed, and the analytes migrated towards the cathode (negative charge) at 20 kV. UV detection was done at 200 nm. Each sample was injected three times for statistical analysis. The replenishment of the BGE was programmed into the method and both BGE vials were replenished before each run to prevent contamination. Peak areas were computed by manual integration in the Agilent OpenLab Software.

4. Results

4.1 Flow Characterization and Monolith Evaluation

For the characterisation of the flow behaviour and for the estimation of physiochemical parameters within the microfluidic channel, flow quantities were calculated based on channel geometry, flow rates

and monolith characteristics. The rectangular channel geometries of both SCC and LCC were confirmed with the Dekttakt XT (Bruker). In Lafleur et al. (2015) and Jönsson et al. (2017) the packing density of the monolith filled channel is stated to be 60% and bead diameter is ~1.4 µm. For calculating the flow resistance and pressure drops, the flow rates of 2 and 10 µL/min were considered. Due to the limited literature on invertase-specific viscosity and that protein solutions often show near-Newtonian behaviour at low to moderate concentrations the viscosity was assumed to be 1 mPa·s at a temperature of 25°C. For the specific formulas and microfluidic theory see Appendix D. For the calculation of the surface coverage of ConA a 1:1 binding ratio was assumed.

Table 1: Flow characteristics calculations; a…Value was calculated with 95% confidence interval

Parameters	**SCC**	**LCC**
Chip dimensions [cm]	2x2	2x2
Channel length [mm]	10	73
Channel width [µm]	500	500
Channel height [µm]	300	175
Cross sectional area [mm^2]	0.15	0.09
Empty channel		
Channel volume [µL]	1.5	6.39
Flow resistance w.o. monolith [Pa·s/m3]	$1.00 \cdot 10^{7}$	$4.20 \cdot 10^{8}$
Pressure drop w.o. monolith (Q=2 µL/min) [mbar]	$4.76 \cdot 10^{-3}$	$13.98 \cdot 10^{-3}$
Pressure drop w.o. monolith (Q=10 µL/min) [mbar]	$23.81 \cdot 10^{-3}$	$69.90 \cdot 10^{-3}$
Reynolds number (Q=2 µl/min)	$83.33 \cdot 10^{-3}$	$98.77 \cdot 10^{-3}$
Reynolds number (Q=10 µl/min)	$416.67 \cdot 10^{-3}$	$493.83 \cdot 10^{-3}$
Monolith-filled channel		
Hydraulic permeability [m^2]	$1.47 \cdot 10^{-8}$	
Flow resistance with monolith [Pa·s/m^3]	$4.54 \cdot 10^{15}$	$5.68 \cdot 10^{16}$
Pressure drop with monolith (Q=2 µL/min) [mbar]	151.17	1891.80
Pressure drop with monolith (Q=2 µL/min) [psi]	21.93	274.38
Pressure drop with monolith (Q=10 µL/min) [mbar]	755.86	9460.12
Pressure drop with monolith (Q=10 µL/min) [psi]	109.63	1371.92
Superficial velocity (Q=2 µL/min) [cm/min]	2.22	3.81
Superficial velocity (Q=10 µL/min) [cm/min]	11.11	19.05
Interstitial velocity (Q=2 µL/min) [cm/min]	3.70	6.35
Interstitial velocity (Q=10 µL/min) [cm/min]	15.52	31.75
Residence time monolith channel (Q=2 µL/min) [s]	27.00	114.97
Residence time monolith channel (Q=10 µL/min) [s]	5.40	22.99
Reynolds number (Q=2 µl/min)	$3.11 \cdot 10^{-4}$	$5.33 \cdot 10^{-4}$
Reynolds number (Q=10 µl/min)	$1.56 \cdot 10^{-3}$	$2.67 \cdot 10^{-3}$
Péclet number (Q=2 µL/min)	9.27	15.89
Péclet number (Q=10 µL/min)	46.35	79.45

Diffusion length distance between monolith beads [µm]	1.18	
Diffusion time [s]	0.02	
Diffusion / Residence ratio (Q=2 µl/min)	$7.69 \cdot 10^{-4}$	$1.81 \cdot 10^{-4}$
Diffusion / Residence ratio (Q=10 µl/min)	$38.46 \cdot 10^{-4}$	$9.03 \cdot 10^{-4}$
Bead calculations and Surface coverage		
Surface area per bead [m^2]	$6.16 \cdot 10^{-12}$	
Volume per bead [m^3]	$1.44 \cdot 10^{-18}$	
Packed bed volume [m^3]	$9.0 \cdot 10^{-10}$	$3.83 \cdot 10^{-9}$
Packed bed volume [µl]	0.9	3.83
Number of beads	$6.26 \cdot 10^{8}$	$2.67 \cdot 10^{9}$
Maximum amount of Inv eluted off [pmol]	15.1	20.1
Surface coverage ConA (max. amount), 1:1 binding ratio, [ng/cm^2]	41.22	12.90
Minimum amount of Inv eluted off [pmol]	7.5	11.2
Surface coverage ConA (min. amount), 1:1 binding ratio, [ng/cm^2]	20.61	7.09
Surface coverage Pepsin (Lafleur et al., 2015) [ng/cm^2]	260±70[a]	

4.2 Binding studies with ConA

Unless otherwise specified, the amount of ConA that was flushed through the chip was 600 µg (~5660 pmol tetramer, 10 mg/mL, 30 min at 2 µL/min).

4.2.1 Proof of concept for ConA binding

To validate the functionality of the ConA-coated microfluidic chip, a series of experiments were conducted to assess the retention and elution of invertase. Initially, flow of invertase through the chip was assessed and compared to the previously collected data from the former student, who conducted the flow through experiment of MαM.

Figure 9A and B represent the MαM concentration in the flow through, binding and elution fractions from two different SCC chips. All steps were done at a flowrate of 15 µL/min and fractions were taken every minute. The loading of MαM is marked with FT (pink). The wash step on the chip is indicated in yellow. In the elution frame (blue), MαM appears in the first elution fraction. The elution was done with 100 mM Acetic Acid.

Figure 9 C represents the flow through of invertase on a LCC (black bars) and a SCC (grey bars). On the LCC, a 1 mg/mL invertase solution was applied at a flow rate of 2 µL/min for 30 min (60 µg, ~3 µM) and then stopped for 30 min for incubation. For the SCC a 0.5 mg/mL invertase solution was flushed through in the same manner. The load, wash and elution were marked in the same colours as for the MαM flow through. The wash after the elution is marked in green. The elution was done with 1 M MαM in MQ water. Figure 9 D shows the electropherograms of the 3 elution fractions of the LCC flow-through and elution profile.

The total amount of analyte loaded onto the system was estimated to be 222 pmol, based on a sample concentration of 1 mg/mL. Analysis of the flow-through fractions of the LCC showed a total of 138 pmol, while the combined elution fractions contained approximately 54 pmol, giving a total recovered amount of around 192 pmol. This suggests that the majority of the analyte could be accounted for, indicating effective binding and elution from the system. In the SCC measurement, the sum of flow-through (80 pmol) and elution fractions (19 pmol) was approximately 99 pmol, which could indicate either sample loss or incomplete recovery under those conditions.

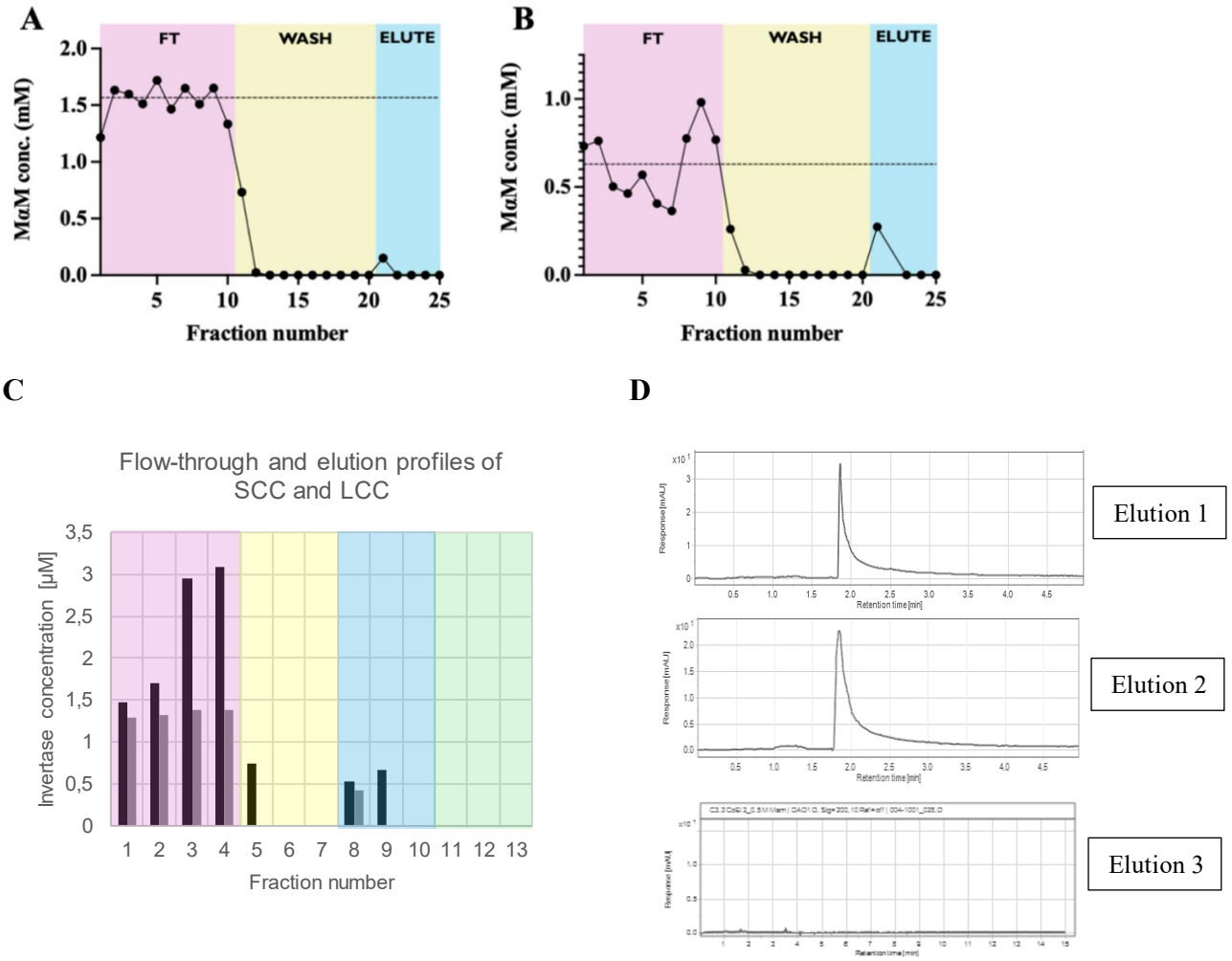

Figure 9: Flow-through and elution profiles to validate the functionality of the ConA-coated microfluidic chip. (A–B): Flow-through experiments of MαM on two different SCC chips at a flow rate of 15 µL/min with 1-minute fraction collection. The loading phase (FT) is shown in pink, the wash step in yellow, and the elution in blue. MαM elutes primarily in the first elution fraction. (C): Flow-through of invertase on an LCC chip (black bars, 1 mg/mL) and an SCC chip (grey bars, 0.5 mg/mL) under low flow and incubation conditions. Fractionation follows the same colour scheme as MαM. Wash after elution is marked in green.
(D): Electropherograms of the three elution fractions from the LCC experiment (black bars, blue section).

4.2.2 Method optimization

Before the quantification of the amount of invertase that was bound onto the functionalised chip, the former protocol was adjusted, and the adjusted steps were tested on SCC. As a reference the commercial HiTrapTM ConA columns from Cytiva were used (*HiTrap™ Con A 4B Columns*, o. D.). The elution

was done with 1 M MαM (in MQ water, 1mM $CaCl_2$, 1mM $MnCl_2$), which appeared to be well suited for electrokinetic injection, due to reproducible signals and low background noise. For detailed protocol, see Appendix B.

Loading buffer

In the former protocol invertase was dissolved in 20 mM citrate buffer, 2 mM $MgCl_2$, 2 mM $MnCl_2$, 2 mM $CaCl_2$, pH 5.2 and loaded on the chip. This was changed to 20 mM TRIS pH 7.5 0.5 M NaCl, 1 mM $MnCl_2$, 1 mM $CaCl_2$, pH 7.5 because of the hypothesis that at a pH of < 6.5 ConA dissociates into a dimer. If the immobilised ConA would disassociate, the not immobilised monomers would be stripped off, resulting into fewer available sites for invertase-binding (one binding site per ConA monomer) (Bouckaert et al., 1995). As can be seen in Figure 10 A this adjustment resulted in higher yield of invertase eluted off on the chip.

Flowrate

In the former protocol the analytes were flushed through the system at 15 µL/min. For testing if binding capacity would increase, the flow rate for invertase loading and elution was set down to 2 µL/min, prolonging incubation time. Further it showed to make the flow through the chip more reproducible. As can be seen in Figure 10 B the chip that was treated with slower flow rates resulted in higher yield of eluted invertase. However, due to the missing of chip replicates, these results have to be treated carefully.

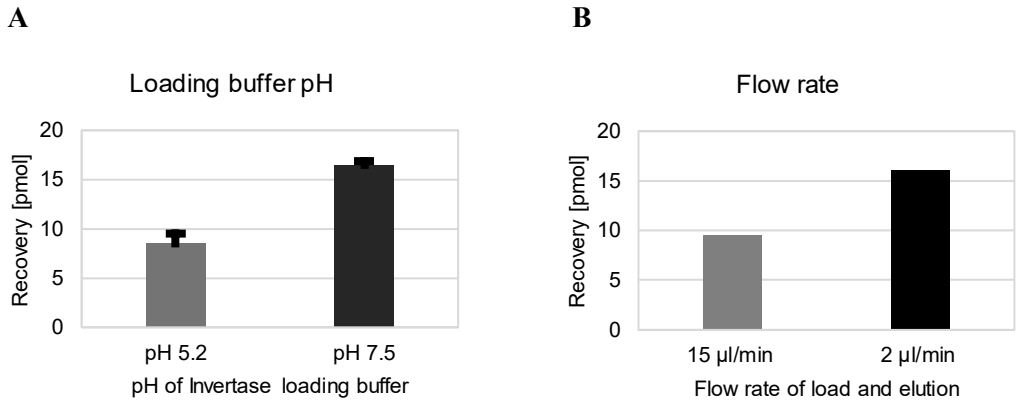

Figure 10: (A): Different amount of invertase [pmol] eluted off the ConA-functionalised chip treated with 2 mg/mL invertase in binding buffer pH 5.1 and pH 7.5. Two SCC for each condition.
(B): Different amount of invertase [pmol] eluted off when load and elute flow rate was set down from 15 µL/min to 2 µL/min. Loading with 2 mg/mL invertase in 20 mM TRIS pH 7.5 0.5 M NaCl, 1 mM MnCl2, 1 mM CaCl2 pH 7.5. One SCC for each condition.

4.2.3 Glycoprotein quantification

To quantify invertase in the elution fractions and to establish the breakthrough curves, calibration curves were run using protein solutions prepared with the same matrixes as the samples, due to the strong matrix effect observed during electrokinetic injection. In Calibration curve (1) (Figure 11 A) invertase was dissolved in MQ water with 1 M MαM, 1mM $CaCl_2$ and 1mM $MnCl_2$. In Calibration curve (2) (Figure 11 E) invertase was prepared in MQ water containing 1 mM $MnCl_2$ and 1 mM $CaCl_2$. Both calibration curves show a strong linear relationship between peak area and invertase concentration.

Figure 11 B and C show the relationship between the amount of eluted invertase (in 45 µL) and the total amount flushed through the chip for both the LCC and SCC in pmol. Due to the occurrence of chip failure and the large time consumption of manufacturing one ConA-functionalised chip, repeating the experiment on multiple chips was sometimes not possible. However, for most of the datapoints, results from 2 to 3 chips that experienced identical conditions, were averaged to ensure the strength of the data point. As can be seen in Figure 11 B and C, both SCC and LCC show a non-linear relation between the yield and the applied amount of invertase. The data were fitted with a logarithmic model, as it yielded the highest R^2 value. However, this does not necessarily imply causation, and the model should be interpreted with caution. Both channel designs resulted in the smallest yield at the lowest used invertase concentration of 0.5 mg/mL (1.85 µM, 60 µL, ~83 pmol). With raising concentration, the amount of recovered invertase increased, both for the LCC and SCC. Figure 11 D directly compares SCC to LCC. To comprehend the binding dynamics of the chip, breakthrough curves were generated using 1 mg/mL invertase solution (60 µg total applied), as shown in Figure 11 F. The flowrate was set to 2 µL/min and the fractions were taken each 7.5 min. These curves were measured for both SCC (grey) and LCC (black).

A

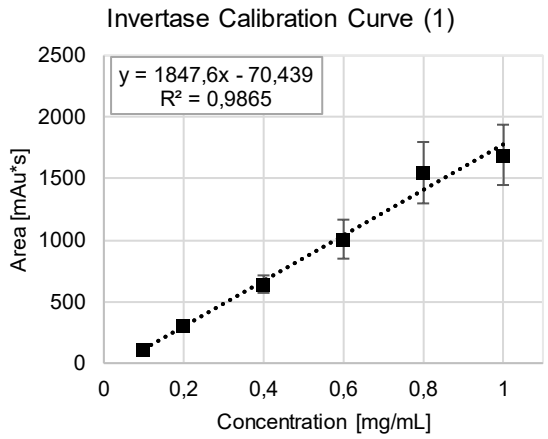

B

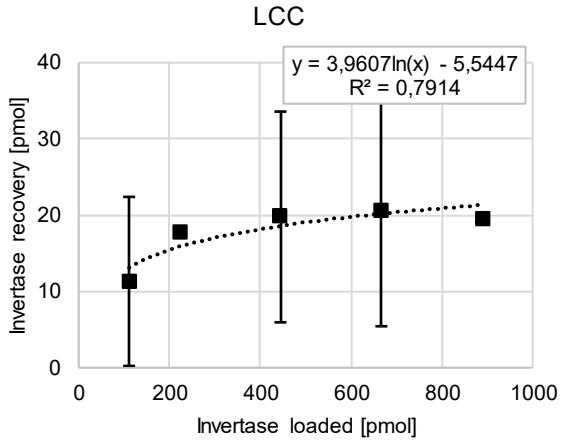

C

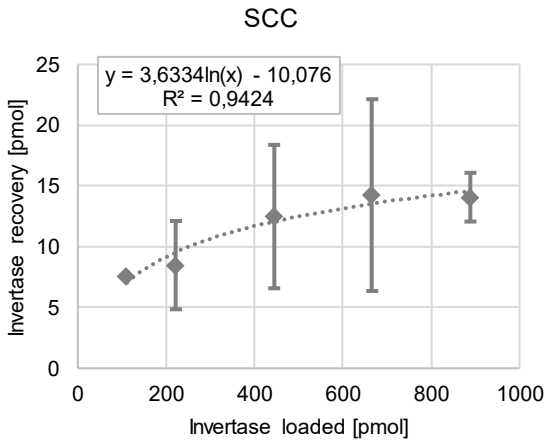

D

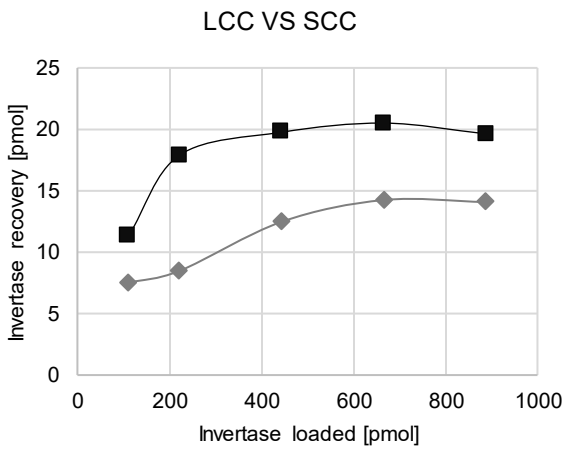

E **F**

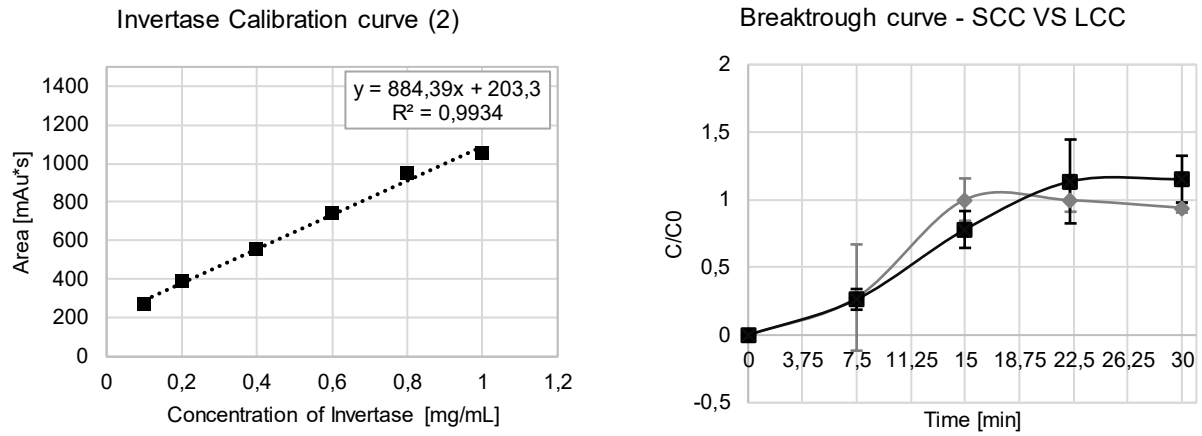

Figure 11: (A): Invertase Calibration curve (1) prepared in MQ water with 1 M MαM. Three independent dilution series were performed with concentrations ranging from 0.1 to 1 mg/mL. Each concentration was measured in triplicate.
(B): Recovered amount of invertase from LCC chips as a function of the total invertase flushed through the chip.
(C): Recovered amount of invertase from LCC chips as a function of the total pmol of invertase flushed through the chip.
(D): Comparison of recovery between SCC and LCC.
(E): Invertase Calibration curve (2) prepared in MQ water with 1 mM $MnCl_2$ and 1 mM $CaCl_2$. Similar to (A), three dilution series were performed (0.1–1 mg/mL), each measured in triplicate. Error bars are too small to be visible.
(F): Breakthrough curves for SCC (grey) and LCC (black) for 1 mg/mL invertase. LCC Data represents the data from three chips that were used for a breakthrough curve. SCC Data represent technical triplicates from a single chip.

4.2.4 Measurement Reproducibility

A total of 36 chips were tested across all concentrations and experimental conditions. Of these, 11 chips failed to produce data, resulting in a failure rate of approximately 30%. Chip failures are defined by missing signals or inconsistent flow that prevented collection of flow fractions. 12 LCC and 24 SCC experiments were conducted. SCC showed a higher failure rate of ~38% than the LCC with ~17% (Appendix C).

As can be seen from Figure 11 B and C, the standard deviations (error bars) of the considered chip results are very broad. The issue of lacking reproducibility was encountered already very early in the project. Thus, to strengthen the data points, the averaging of data from multiple chip replicates was very important. The technical replications (three CE-UV measurements per sample) showed relatively low variability.

4.2.5 Chip Reusability

To explore if the chips were reusable, the regeneration steps were done, and the chips were stored at 4°C in glucose-containing buffer overnight. The second experiments were carried out under the same conditions as the first ones, including that the same amount of moles of invertase were flushed through the chips. In Figure 12 the amount of invertase eluted of SCC and LCC in first and second experiment

are compared to each other. As can be seen, for both channel designs the amount of recovered invertase is lower in the second than in the first experiment.

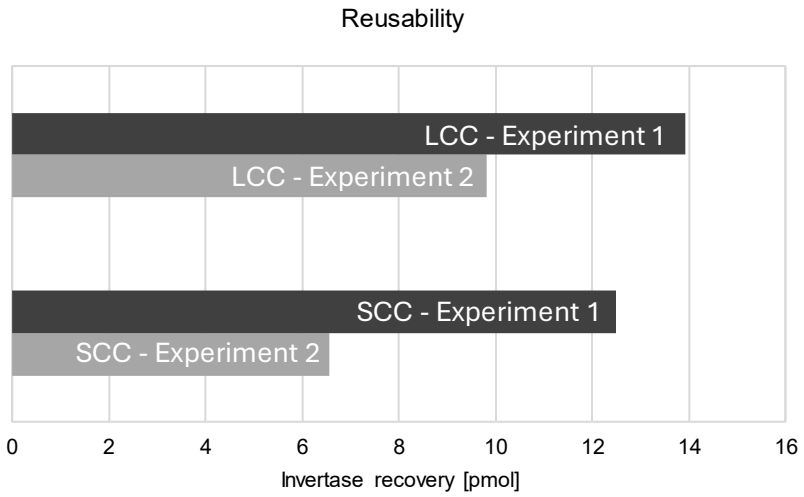

Figure 12: Assessment of reusability of SCC and LCC. 2 mg/mL (120 µg) of invertase were loaded onto the chip.

5. Discussion

5.1 Theoretical calculations

The values that were obtained through the calculations and estimations give a broad overview of fluid behaviour, provide an idea on binding capacity, biochemical characteristics and help to compare the performance of SCC and LCC.

The introduction of a monolith structure with an estimated packing density of 60% (Jönsson et al., 2017) and a bead diameter of ~1.4 µm (Jönsson et al., 2017) significantly increased the flow resistance by a magnitude of 10^4 for SCC and LCC, possibly due to reduced void volume and tortuosity. The increased flow resistance also resulted in a higher pressure drop in both SCC and LCC compared to the absence of monolith and highlights the significant differences between the channel designs. The monolith-filled SCC shows a pressure drop of 151.17 mbar at 2 µL/min and 755.86 mbar at 10 µL/min (22 and 110 psi). The monolith-filled LCC exhibits a pressure drop of 1891.80 mbar at 2 µL/min and 9460.12 mbar at 10 µL/min (275 and 1372 psi). As has been reported in Jönsson et al. (2017) the monolith structure loses mechanical stability at a pressure over 500 psi, which makes the flowrate of 10 µL/min not applicable for the monolith-filled LCC design.

The Reynolds numbers for both monolith-occupied SCC and LCC were below 1 (0.08, 0.42), indicating laminar flow through the porous structure, even at a higher flowrate of 10 µL/min.

5.2 Binding evaluation

As shown in Figure 9 A-C the flow through behaviour of MαM matches the behaviour of invertase. Although the flow conditions, elution methods, applied analyte concentrations/amounts and detection

method were different, in all cases the analyte of interest could be detected in the elution fractions. This strengthens the hypothesis that the immobilised ConA is active and thus able to bind complex and simple carbohydrate structures.

The asymmetric peak shape of the protein separation in the CE can be seen in Figure 9 D. The occurrence of peak tailing could be due to heterogeneity of the glycoprotein forms. Due to the LPA-coating, the absorption to the capillary wall is less probable, but could contribute as well.

5.3 Optimization and Method Performance

As can be seen in Figure 10 A the pH of the invertase loading buffer appears to have an impact on the yield of invertase eluted off the chip. The use of a 20 mM Tris buffer pH 7.5 seems to result in a higher yield of invertase, than a 20 mM Ammonium acetate buffer pH 5.2.

Invertase has its isoelectric point around 4.5, thus it carries a net negative charge at pH 7.5. This enhances solubility and reduces aggregation, which could make more binding residues available for ConA-interaction. ConA adopts its active tetrameric form around pH 7 and tends to dissociate into its dimeric form at pH < 6.5. Thus, the pH could affect both ligand (invertase), by enhancing solubility and lectin, by favouring the optimal binding conformation.

An experiment was conducted that assesses the flow rates effect on the yield of invertase and the outcome can be seen in Figure 10 B. The application of lower flow rates for loading and elution appeared to increase the amount of eluted off invertase. The residence time of the analyte is indirectly dependent on the volumetric flow rate. Thus, decreasing the flow rate for the invertase loading increases the time that the glycoprotein can interact with the immobilised ConA.

Similarly, during elution, a slower flow rate allows longer time for the competition for the binding sites, which would result in a higher amount of recovered protein. As mentioned in the introduction, the association constants for ConA-monosaccharide interaction are relatively low, which makes flow control and residence time important factors to reach binding equilibrium.

To underline this, the residence time in the monolith-filled SCC was calculated for 2 µL/min and 10 µL/min to be 27 and 5.4 s, respectively. This overlaps with the findings of Jönsson et al., 2017. The estimated diffusion coefficient for invertase, with an assumed hydrodynamic radius of 4.3 nm, is $3.35 \cdot 10^{-11}$ m^2/s. In the monolith-filled channel the diffusion distance between particles was estimated to be 1.18 µm, which would imply a diffusion time of 0.02 s between the monolith beads (see Appendix C).

The estimated Péclet numbers for invertase indicate that advection (transport-driven flow) dominates over diffusion in both monolith-filled channel designs with values ≥ 10. At 2 µL/min, the Péclet numbers are approximately 9.3 and 15.9, while at 10 µL/min, they rise to around 46.3 and 79.4, for SCC and LCC respectively. This roughly fivefold increase corresponds directly to the fivefold increase in flow rate, as the Péclet number scales linearly with velocity. The higher Péclet numbers at increased flow rates strengthen that advective transport becomes more dominant. These results highlight how strongly

mass transport behaviour is influenced by flow conditions. Thus, the flow stop for incubation would provide time for axial dispersion via diffusion.

5.4 Analysis of Quantification and Recovery

This work aimed to evaluate the chip performance by analysing the effect of different loading concentrations on recovery to test the capacity limit of the chip. The elution yield of invertase of SCC and LCC displayed a non-linear relationship with input concentration, revealing two distinct trends: a drop in recovery at low concentrations and a potential saturation effect at higher levels (Figure 11 B and C).

5.4.1 Low concentration binding inefficiency

Notably, even at the lowest tested concentration, the total number of invertase molecules introduced exceeded the number recovered. This could indicate that the loss in yield cannot be solely explained by insufficient invertase availability. One plausible explanation is reduced binding efficiency at lower concentrations due to decreased interaction frequency between invertase and the ConA-coated surface. Additionally, at these low concentrations, multivalency effects may intensify. Enhanced avidity through the cluster glycoside effect, may result in stronger retention, which is harder to reverse during elution, particularly when using mannose for competitive elution.

The kinetics of invertase binding to ConA are challenging to define due to the complex and heterogeneous glycosylation patterns of the enzyme. Unlike monosaccharide ligands, invertase presents a dense and multivalent structure of N-linked glycans that can simultaneously interact with multiple ConA binding sites. This multivalency complicates the estimation of a clear association (K_A) and dissociation (K_D) rate constant. However, comparative insights can be drawn from structurally similar carbohydrate ligands. Glycogen, a densely branched glucose polymer, binds to ConA with significantly higher affinity than mannan. In Coulibaly & Youan (2014) the ConA-polysaccharide association and dissociation constants are reported to be $K_A = \sim 4 \cdot 10^6\ M^{-1}$ and $K_D = \sim 0.3\ \mu M$. In contrast the ConA to mannan association and dissociation constants are stated to be $K_A = \sim 3.5 \cdot 10^5\ M^{-1}$ and $K_D = \sim 3\ \mu M$. In this publication it is discussed that glycoproteins with branched high-mannose structures (like invertase) may form relatively stable complexes with ConA, potentially leading to lower dissociation rates (Coulibaly & Youan, 2014).

If due to the multivalent nature of invertase its dissociation constant is low, this implies tight binding and raises the possibility of rate-limiting elution. Such strong retention could hinder the competitive displacement by MαM. Especially in flow-through systems, rapid transit times may not be sufficient for complete equilibration, meaning that association kinetics could also become limiting at low invertase concentrations.

5.4.2 Impact of sample heterogeneity

The chips were tested with 'Invertase from baker′s yeast (*S. cerevisiae*)', which presumably is a heterogenous mix of glycosylated to non-glycosylated form (Product information, Sigma-aldrich n.d.). The product description did not specify the ratio or purification procedure. Depending on the purification process, commercial invertase is typically a heterogeneous mixture of a glycosylated and non-glycosylated form. In the used CE separation method, these two forms could not be distinguished and thus the standard curve is conducted with this mixture. However, the protein recovery percentage off the chip is mostly around 2-5%, thus the impurity of the invertase standard is probably not the main limitation of the elution yield.
Saleemuddin et al. (1991) declares that the purity of the glycoprotein appears to have no significant effect on the complex formation with the lectin. However, for future quantitative testing of this system, it would be beneficial to use a well-defined and purified glycoprotein standard.

5.4.3 Plateau at high invertase concentrations

At higher input from 2 to 4 mg/mL, the observed yield began to plateau despite the increased number of invertase molecules introduced. This plateauing effect was observed across replicates. This is likely limited by ConA density and steric accessibility within the monolith structure. As a reference, it has been reported by Jönsson et al. (2017) that approximately 6 ± 1 µg of pepsin (~34 kDa, Bougatef et al., 2007), corresponding to ~173.91 pmol, can be immobilized on a chip with geometries comparable to the SCC.

The actual ConA density on the monolith surface may be lower than the theoretical maximum due to missing surface characterization data. Due to the larger hydrodynamic radius of ConA compared to pepsin, the lectin may sterically occupy multiple attachment sites, reducing the moles of immobilised ConA. The ratio between the hydrodynamic radii of ConA tetramer and pepsin is 1.3 (4.3/3.4 nm) (Gtari et al., 2016), (Durchschlag et al., 1997). This size difference could explain why fewer moles of ConA are immobilized on the monolith than theoretically expected. Estimation of the occupied surface area suggests that one ConA protein occupies 1.6x more surface area than one pepsin molecule. If an assumed amount of 173.91 pmol pepsin can be immobilised on an SCC-like chip, the maximum expected amount of ConA (106 kDa) is 109.4 pmol, which corresponds to ~11.6 µg. This still exceeds the average maximum amount of invertase (15.1 pmol) eluted off the SCC by roughly a factor of 7.

Recovery limitations could also be due to mass transfer limitations or binding kinetics. The effect of multivalency on binding kinetics is discussed above. The estimated Péclet numbers for both channels suggest that at the flow rate of 2 µL/min, convection dominates over diffusion. Invertase is a very large molecule and thus has a low diffusion constant. This problem was tackled by stopping the flow for incubation (see Appendix B). Although the monolith architecture reduces diffusion distances due to its porous and high surface area structure, fast flow and the large size of invertase (~270 kDa, Product

Information, Sigma-aldrich n.d.) may still cause transport limitation. This is supported by the system's behaviour at fast flow rates, suggesting that the invertase proteins may not efficiently reach all ConA binding sites before exiting the monolith-filled channel.

5.4.4 The breakthrough curves and chip capacity estimation

To determine the absorption capacity of the chip and the mass transfer characteristics, breakthrough curves were conducted. The curve shape depends on mass transfer effects as well as association rates of invertase to ConA. When absorption rates are very low and mass transfer is slow, breakthrough curves become flatter. A flat curve shows that the analyte goes through the channel without interaction. (*Kinetics, Dynamic Sorption,* DynaSorb BT, Accessed on 02.06.2025).

For both SCC and LCC the breakthrough curves appear to be relatively flat in Figure 11 F. The effects of mass transfer and binding kinetics has been elaborated on in 4.1.1. However, the absence of a sharp step function in both SCC and LCC breakthrough curves could also be due to the relatively large sample size (15 µL). This may explain why protein is already detected in the first fraction, as the current sampling method lacks sufficient resolution to distinguish small concentration changes and misses the breakthrough point. For future investigation NanoDrop measurements would be more appropriate, as they allow high-sensitivity analysis of smaller sample volumes, providing better temporal resolution and a more accurate representation of protein breakthrough behaviour.

The breakthrough curves of both the SCC and LCC indicate that for a 1 mg/mL invertase solution, saturation is reached after approximately 15 min, with the breakthrough point occurring before 7.5 min. A 7.5 min invertase flow through corresponds to 15 µL of the 1 mg/mL invertase solution, which contains roughly 56 pmol. The maximum amount that was retained on the chip was around 15 and 20 pmol, for SCC and LCC respectively.

5.4.5 Comparison of SCC and LCC performance

Comparative analysis (Figure 11 D) shows that the LCC consistently results in higher invertase recovery than the SCC, suggesting that the channel design significantly influences the recovery. The LCC's increased surface area likely promotes more ConA immobilisation. The longer residence time promotes axial dispersion and thus glycoprotein-lectin interaction and elution efficiency.

However, LCC does not outperform SCC as expected. The LCC channel has 7x the length and 4.3x the inner volume of the SCC channel and thus should result in at least double the amount of recovered invertase. The highest recovered invertase amount of the LCC was 20.1 pmol and of SCC was 15.1 pmol, which differs by a factor of only 1.3.

The amount of ConA flushed through the chip was the same for both channel designs and was applied at very high concentration. Also, both show a saturation effect of recovery at increasing invertase concentrations. This suggests that the LCC was probably not limited by the availability of ConA binding sites. In both cases the binding capacity seems to be reached rapidly.

The pressure drop at 10 µL/min flowrate, was calculated to be high enough to disrupt the monolith structure inside the channel (> 500 psi), leaving fewer binding functionalities for ConA immobilisation. However, there was no monolith deformation noted in any of the LCC after the experiment runs.

This would also explain the lower theoretical surface coverage of LCC compared to SCC. Due to the larger volume, the LCC would suggestibly have a larger surface area, thus more ConA and a higher recovery yield of invertase. However, it appears that SCC has a higher surface coverage of 41.22 ng/cm^2 than LCC with 12.90 ng/cm^2. These values for LCC could also indicate the destruction of the monolith structure at higher flow rates. For comparison, Jönsson et al. (2017) reported a surface coverage of ~260 ng/cm^2 of pepsin on an SCC-similar design.

This highlights that the channel design must be considered a critical optimization parameter. The SCC shows less recovery but may offer better pressure control, faster operation and a higher surface coverage, making it the better choice for this microfluidic platform.

5.5 Analysis of Chip Reusability

As can be seen in Figure 12 the full regeneration of both SCC and LCC could not be achieved. With both channel designs the second experiment results in lower yield than the first run. One possible reason for the non-reproducible results in the second experiment could be that ConA detaches from the surface, disassociates or desaturates either under experiment conditions or during storage between the experiments. The ConA functionalized chip was always kept on ice or at 4°C, trying to prevent denaturation. Another reason could be that the regeneration step was not effective enough due to too short incubation time. At alkaline pH, MαM- and protein–lectin interactions weaken because of the change in ionization. This can reduce electrostatic and hydrogen bonding interactions between the glycan and ConA. This gently strips off the bound glycoprotein or MαM. However, some MαM may stay bound and block potential binding sites for the invertase protein during reuse.

Further, the re-equilibration buffer contains a 2% glucose concentration, to ensure ConA binding site stability overnight (Saleemuddin, 1999). This protective ligand may block binding sites for the glycoprotein, reducing the amount invertase that can be bound. However, due to its multivalent character and high mannose cluster, invertase will most likely strongly compete.

5.6 Reliability

The error bars in Figure 11 B and C reflect the standard deviation between the replicate chips. It seems that the variation between the chips is very high, both for SCC and LCC.

There is a possibility that the variability of the measurements can be attributed to the CE method. CE separations are known to have variability between runs. It was aimed to be minimized by the LPA-coating of the capillary, which should result in more consistent runs. Due to the strong dependence of the electrokinetic injection on sample matrix composition, it cannot be neglected that through small differences in ionic strength in the sample fraction, the measurement is not as robust as with

hydrodynamic injection. However, the standard curve showed very repeatable peak areas and migration times.

Variability between the chips may also arise due to monolithic heterogeneity, that can be based on differences in packing density, bead and pore size and polymerisation efficiency. This affects the surface area that is available for ConA immobilisation and consequently the yield of eluted invertase. Another factor that could contribute to the irregularity between chip results is the amount of active ConA that is immobilised.

Other factors that can influence the outcome of the chips are sample handling, including degradation of invertase, and human error. Chip failure due to clogging or flow irregularities might be prevented by filtering the buffers and solutions prior to injecting them onto the chip.

6. Conclusion

This work demonstrates the attempt to characterise the potential of a ConA-functionalised monolithic chip for glycoprotein separation. It highlights the several challenges and 'black boxes' of the system, that must be addressed to optimize chip performance.

The overall goal was to establish, reassure the proof-of-concept and critically assess the chip performance across channel geometry, capacity, reusability and analytical reproducibility. Theoretical calculations helped to understand the impact of fluid flow parameters on mass transfer in the monolith-filled channel. The results of the calculations suggest that advection dominated the transport in the monolithic-filled chip, emphasizing the use of appropriate flow rates and channel geometry. It also suggested that the SCC is more practical than the LCC when it comes to flow rates and pressure drops.

Although the immobilization of ConA was confirmed, the binding capacity of both chip designs were lower than expected. This could be likely due to steric hindrance and the multivalency of both ConA and invertase. LCC outperformed SCC in terms of glycoprotein recovery, possibly due to larger surface area and longer residence times. However, the improvement was not as pronounced as expected. This could be due to the higher theoretical pressure drops in the longer channel affecting the monolith stability and thus immobilisation site availability. This may limit the effective use of the additional surface area in the LCC.

Testing the ability to regenerate the channel surface indicated that the chips do not result in reproducible yields upon reuse. The second experiments with both channel designs, produced lower invertase recovery, possibly due to incomplete removal of invertase and MαM or loss of ConA activity during experimental run or storage. Both instrumental factors, such as electrokinetic injection variability in CE– and chip-related matters like monolith heterogeneity, surface functionalisation and ConA immobilisation efficiency could cause the high variability between chip replicates.

Overall, this work provides an insight into glycoprotein retention on the ConA-functionalised TE monolith, an estimation of binding capacity and a foundation for further development of this lectin-affinity microfluidic device.

7. Future Perspectives

A logical step to assess the amount of ConA immobilised on the chip would be to mark ConA with a fluorescence tag. This would give valuable insights in the immobilisation efficiency and when correlated with glycoprotein recovery, it would also provide an idea of how many immobilised ConA proteins are able to bind glycoprotein. An alternative would be to fluorescently tag the ligand, like in Selzer et al. (2022), where the competitive binding between the fluorescently tagged dextran and glucose was investigated via titration experiments. Another method for quantifying the immobilised ConA is demonstrated in Jönsson et al. (2017). Here, the monolith channel was filled with the protein that should be immobilised (pepsin) and the non-bound proteins were washed off. The sample size was small and measured using NanoDrop technology. To improve the reliability of the system, it should be investigated how reproducible the immobilisation quantity is.

Future work could focus on optimizing the downstream analysis method for protein separation and analysis. To use Mass Spectrometry instead of UV detection would provide structural information and enhance the applicability of this microfluidic system.

Another direction for development involves the application of alternative lectins to expand selectivity of the chip. To create this microarray, the monolith production in the channel could be exploited, by masking distinct channel parts from the UV light. This would create monolith patches, which could each be functionalised with a different kind of lectin. In Zhang et al. (2016) an example of such a microarray with 46 different lectins is described. This array provides a detailed analysis of various glycosylation type abundance in a sample. However, to implement the use of multiple lectins on this projects chip would take considerable optimization efforts, probably a different chip design and the investigation in immobilisation efficiencies and suiting elution strategies for all selected lectins.

In the future, it may be beneficial to test the extraction of glycoproteins from more complex sample matrices to assess its utility in, for example, clinical settings, bioprocess control or environmental studies. The specialisation of the chip protocol and sample matrix must be done accordingly.

Furthermore, it would be beneficial to automate sample injection and washing steps with an injection valve. Although this was considered during this work, it was not fully implemented, due to a need for flexibility for changing the flow. Challenging steps in the flow protocol e.g. increase of viscosity with protein solutions and chip blockage made the full automatization unsuitable. However, the incorporation of an injection system would help minimize human error and prevent the detachment of the channel from the tubing.

Mathematically modelling the process in the packed bed would give complementary information and would help interpret the experimental results. Developing a reactive transport model, that combines mass transport phenomena, fluid flow and binding kinetics would be a suitable approach. It could be used to simulate breakthrough curves and concentration profiles, which would help optimizing the system in regard to elution strategies, injection conditions and channel geometries. Overall, it would offer a powerful tool for the deeper understanding of the underlying extraction mechanism of the chip.

In summary there are many opportunities for this system. One of the most urgent points to consider is finding the point of most variability and optimize the system so it gives reliable and repeatable results. Then the expansion of the system in regard to alternative lectins used and further specialisation depending on the field of application can be done. Overall, this work presents a proof-of-concept aspect of this novel approach of the immobilisation of a non-enzymatic protein on a thiol-ene monolith.

Acknowledgements

The work for this thesis was carried out in the Microscale Analytical Systems laboratory, Department of Pharmacy, Faculty of Health and Medical Sciences, University of Copenhagen from January 2025 to June 2025.

I would like to thank Jörg P. Kutter for supervising me and for the fruitful discussions we had every Friday. He taught me to make systematic changes in the system and that things that may seem easy on first sight, can be very complex and unforeseeable. He left me room to do my independent experiment decisions but always took the time to bounce ideas.

Aoife McLoughlin was a great lab mate and gave me a very good introduction into the project. She was very inspiring, and I want to thank her for being so helpful and welcoming.

Also, I want to thank Anna Nguyen for being so motivating and encouraging. She was an inspiring support, which greatly motivated me throughout the course of this research.

Further I would like to thank Nickolaj Petersen for helping me with the CE set up and always being there for me to test my ideas and give improvement suggestions. It was always lovely to have him around.

Thanks also to Johan Nilsson for overtaking the role of my supervisor at LTH. He is an inspiration.

I would also like to give my thanks to the Protein Analysis Group for creating a wonderful social environment, by always sitting together and having lunch. I want to directly thank Sofia, Paulina, Victor and Omid for being amazing role models and great lab mates. Especially chatting with Jordan often made my day. I am very grateful for his help.

Further, I am very thankful for the support from Dean, who always made me feel great. Thanks also to my close friends Sarah, Patrik, Mikael and Thomas for their support and cheerfulness.

References

Altria, K. D. (2003). Fundamentals of Capillary Electrophoresis Theory. *Humana Press eBooks*, 3–14. https://doi.org/10.1385/0-89603-315-5:3

Andrasi, M., Zagyi, B. & Hamidli, N. (2023). Study of Effect of Incubation Time and Temperature on the Linear Polyacrylamide-Coating Performance for the Separation of Proteins by Capillary Zone Electrophoresis. *Chromatographia*, *86*(10), 659–668. https://doi.org/10.1007/s10337-023-04276-x

Ashwell, G. & Morell, A. G. (1977). Membrane glycoproteins and recognition phenomena. *Trends in Biochemical Sciences*, *2*(4), 76–78. https://doi.org/10.1016/0968-0004(77)90041-x

Bangarh, R., Khatana, C., Kaur, S., Sharma, A., Kaushal, A., Siwal, S. S., Tuli, H. S., Dhama, K., Thakur, V. K., Saini, R. V. & Saini, A. K. (2023). Aberrant protein glycosylation: Implications on diagnosis and Immunotherapy. *Biotechnology Advances*, *66*, 108149. https://doi.org/10.1016/j.biotechadv.2023.108149

Barkai-Golan, R., Mirelman, D. & Sharon, N. (1978). Studies on growth inhibition by lectins of penicillia and aspergilli. *Archives Of Microbiology*, *116*(2), 119–124. https://doi.org/10.1007/bf00406026

Bosques, C. J., Raguram, S. & Sasisekharan, R. (2006). The sweet side of biomarker discovery. *Nature Biotechnology*, *24*(9), 1100–1101. https://doi.org/10.1038/nbt0906-1100

Bouckaert, J., Loris, R., Poortmans, F. & Wyns, L. (1995). Crystallographic structure of metal-free concanavalin A at 2.5 Å resolution. *Proteins Structure Function And Bioinformatics*, *23*(4), 510–524. https://doi.org/10.1002/prot.340230406

Bougatef, A., Balti, R., Zaied, S. B., Souissi, N. & Nasri, M. (2007). Pepsinogen and pepsin from the stomach of smooth hound (Mustelus mustelus): Purification, characterization and amino acid terminal sequences. *Food Chemistry*, *107*(2), 777–784. https://doi.org/10.1016/j.foodchem.2007.08.077

Brewer, C. F., Brown, R. D. & Koenig, S. H. (1983). Metal Ion Binding and Conformational Transitions in Concanavalin A: A Structure-Function Study. *Journal Of Biomolecular Structure And Dynamics*, *1*(4), 961–997. https://doi.org/10.1080/07391102.1983.10507497

Carlborg, C. F., Haraldsson, T., Öberg, K., Malkoch, M. & Van der Wijngaart, W. (2011). Beyond PDMS: off-stoichiometry thiol–ene (OSTE) based soft lithography for rapid prototyping of microfluidic devices. *Lab On A Chip*, *11*(18), 3136. https://doi.org/10.1039/c1lc20388f

Chu, F. K., Watorek, W. & Maley, F. (1983). Factors affecting the oligomeric structure of yeast external invertase. *Archives Of Biochemistry And Biophysics*, *223*(2), 543–555. https://doi.org/10.1016/0003-9861(83)90619-7

Cobb, K. A., Dolnik, V. & Novotny, M. (1990). Electrophoretic separations of proteins in capillaries with hydrolytically-stable surface structures. *Analytical Chemistry*, *62*(22), 2478–2483. https://doi.org/10.1021/ac00221a013

Coelho, L. C. B. B., Silva, P. M. D. S., De Menezes Lima, V. L., Pontual, E. V., Paiva, P. M. G., Napoleão, T. H. & Correia, M. T. D. S. (2017). Lectins, Interconnecting Proteins with Biotechnological/Pharmacological and Therapeutic Applications. *Evidence-based Complementary And Alternative Medicine*, *2017*(1). https://doi.org/10.1155/2017/1594074

Courtois, J., Szumski, M., Byström, E., Iwasiewicz, A., Shchukarev, A. & Irgum, K. (2006). A study of surface modification and anchoring techniques used in the preparation of monolithic microcolumns in fused silica capillaries. *Journal Of Separation Science*, *29*(1), 14–24. https://doi.org/10.1002/jssc.200500294

Da Silva, C. P., De Queiroz, T. G. A., Nogi, K. I., Katz, I. S. S., Guedes, F., Fernandes, E. R., Silva, K. R. & Silva, S. R. (2024). Analysis of the antigenic and immunogenic properties of the native rabies virus glycoprotein purified by Lens culinaris lectin affinity chromatography. *Journal Of Virological Methods*, *331*, 115044. https://doi.org/10.1016/j.jviromet.2024.115044

Dam, T. K., Roy, R., Das, S. K., Oscarson, S. & Brewer, C. (2000). Binding of Multivalent Carbohydrates to Concanavalin A andDioclea grandiflora Lectin. *Journal Of Biological Chemistry*, *275*(19), 14223–14230. https://doi.org/10.1074/jbc.275.19.14223

Dixit, C. K. (2022). Ligand Immobilization Methods for Affinity Chromatography. *Methods in Molecular Biology*, 241–247. https://doi.org/10.1007/978-1-0716-2176-9_16

Durchschlag, H., & Zipper, P. (1997). Calculation of hydrodynamic parameters of biopolymers from scattering data using whole-body approaches. In *Analytical Ultracentrifugation IV* (pp. 43-57). Steinkopff.

Fujiwara, Y., Tanno, Y., Sugishita, H., Kishi, Y., Makino, Y. & Okada, Y. (2021). Preparation of optimized concanavalin A-conjugated Dynabeads® magnetic beads for CUT&Tag. *PLoS ONE*, *16*(11), e0259846. https://doi.org/10.1371/journal.pone.0259846

Goldstein, I. J., Hollerman, C. E. & Smith, E. E. (1965). Protein-Carbohydrate Interaction. II. Inhibition Studies on the Interaction of Concanavalin A with Polysaccharides*. *Biochemistry*, *4*(5), 876–883. https://doi.org/10.1021/bi00881a013

Goumenou, A., Chendo, C., Combès, A., Fournier, T., Pichon, V. & Delaunay, N. (2024). Characterization of Concanavalin A-based lectin sorbents for the extraction of the human chorionic gonadotropin glycoforms prior to analysis by nano liquid chromatography-high resolution mass spectrometry. *Journal Of Pharmaceutical And Biomedical Analysis*, *242*, 116022. https://doi.org/10.1016/j.jpba.2024.116022

Gtari, W., Bey, H., Aschi, A., Bitri, L. & Othman, T. (2016). Impact of macromolecular crowding on structure and properties of pepsin and trypsin. *Materials Science And Engineering C*, *72*, 98–105. https://doi.org/10.1016/j.msec.2016.11.046

Hajba, L. & Guttman, A. (2017). Recent advances in column coatings for capillary electrophoresis of proteins. *TrAC Trends in Analytical Chemistry*, *90*, 38–44. https://doi.org/10.1016/j.trac.2017.02.013

Hamblin, J. & Kent, S. P. (1973). Possible Role of Phytohaemagglutinin in Phaseolus vulgaris L. *Nature New Biology*, *245*(140), 28–30. https://doi.org/10.1038/newbio245028a0

Hamidli, N., Andrasi, M., Nagy, C. & Gaspar, A. (2021). Analysis of intact proteins with capillary zone electrophoresis coupled to mass spectromery using uncoated and coated capillaries. *Journal Of Chromatography A*, *1654*, 462448. https://doi.org/10.1016/j.chroma.2021.462448

Hamilton, S. R. & Gerngross, T. U. (2007). Glycosylation engineering in yeast: the advent of fully humanized yeast. *Current Opinion in Biotechnology*, *18*(5), 387–392. https://doi.org/10.1016/j.copbio.2007.09.001

Hassing, G. S. & Goldstein, I. J. (1970). Ultraviolet Difference Spectral Studies on Concanavalin A. *European Journal Of Biochemistry*, *16*(3), 549–556. https://doi.org/10.1111/j.1432-1033.1970.tb01116.x

He, M., Zhou, X. & Wang, X. (2024). Glycosylation: mechanisms, biological functions and clinical implications. *Signal Transduction And Targeted Therapy*, *9*(1). https://doi.org/10.1038/s41392-024-01886-1

Hefnawy, M., El-Gendy, M., Al-Salem, H., Marenga, H., El-Azab, A., Abdel-Aziz, A., Gamal, A. E., Alanazi, M., Obaidullah, A., Al-Hossaini, A. & Hefnawy, A. (2023). Trends in monoliths: Packings, stationary phases and nanoparticles. *Journal Of Chromatography A*, *1691*, 463819. https://doi.org/10.1016/j.chroma.2023.463819

Hillmering, M., Pardon, G., Vastesson, A., Supekar, O., Carlborg, C. F., Brandner, B. D., Van der Wijngaart, W. & Haraldsson, T. (2016). Off-stoichiometry improves the photostructuring of thiol–enes through diffusion-induced monomer depletion. *Microsystems & Nanoengineering*, *2*(1). https://doi.org/10.1038/micronano.2015.43

HiTrap™ Con A 4B columns. (o. D.). https://www.cytivalifesciences.com/en/us/shop/chromatography/prepacked-columns/affinity-specific-groups/hitrap-con-a-4b-columns-p-05309

Janzen, D. H., Juster, H. B. & Bell, E. A. (1977). Toxicity of secondary compounds to the seed-eating larvae of the bruchid beetle Callosobruchus maculatus. Phytochemistry, 16(2), 223–227. https://doi.org/10.1016/s0031-9422(00)86790-4

Jönsson, A., Svejdal, R. R., Bøgelund, N., Nguyen, T. T. T. N., Flindt, H., Kutter, J. P., Rand, K. D. & Lafleur, J. P. (2017). Thiol-ene Monolithic Pepsin Microreactor with a 3D-Printed Interface for Efficient UPLC-MS Peptide Mapping Analyses. *Analytical Chemistry*, *89*(8), 4573–4580. https://doi.org/10.1021/acs.analchem.6b05103

Kalb, A. J. & Levitzki, A. (1968). Metal-binding sites of concanavalin A and their role in the binding of α-methyl d-glucopyranoside. *Biochemical Journal*, *109*(4), 669–672. https://doi.org/10.1042/bj1090669

Kinetics | Dynamic Sorption, Breakthrough Curve Measurement, MixSorb, DynaSorb BT. (o. D.). https://www.dynamicsorption.com/dynamic-sorption-method/kinetics/

Kissel, T., Toes, R. E. M., Huizinga, T. W. J. & Wuhrer, M. (2022). Glycobiology of rheumatic diseases. *Nature Reviews Rheumatology*, *19*(1), 28–43. https://doi.org/10.1038/s41584-022-00867-4

Kuno, A., Uchiyama, N., Koseki-Kuno, S., Ebe, Y., Takashima, S., Yamada, M. & Hirabayashi, J. (2005). Evanescent-field fluorescence-assisted lectin microarray: a new strategy for glycan profiling. *Nature Methods*, *2*(11), 851–856. https://doi.org/10.1038/nmeth803

Lafleur, J. P., Senkbeil, S., Novotny, J., Nys, G., Bøgelund, N., Rand, K. D., Foret, F. & Kutter, J. P. (2015). Rapid and simple preparation of thiol–ene emulsion-templated monoliths and their application as enzymatic microreactors. *Lab On A Chip*, *15*(10), 2162–2172. https://doi.org/10.1039/c5lc00224a

Lee, R. T. & Lee, Y. C. (2000). Affinity enhancement by multivalent lectin-carbohydrate interaction. *Glycoconjugate Journal*, *17*(7/9), 543–551. https://doi.org/10.1023/a:1011070425430

Lis, H. & Sharon, N. (1998). ChemInform Abstract: Lectins: Carbohydrate-Specific Proteins that Mediate Cellular Recognition. *ChemInform*, *29*(25). https://doi.org/10.1002/chin.199825333

Locke, A. K., Cummins, B. M., Abraham, A. A. & Coté, G. L. (2014). PEGylation of Concanavalin A to Improve Its Stability for an In Vivo Glucose Sensing Assay. *Analytical Chemistry*, *86*(18), 9091–9097. https://doi.org/10.1021/ac501791u

Mariño, K., Bones, J., Kattla, J. J. & Rudd, P. M. (2010). A systematic approach to protein glycosylation analysis: a path through the maze. *Nature Chemical Biology*, *6*(10), 713–723. https://doi.org/10.1038/nchembio.437

McLoughlin, A. (n.d.). *Development of a lectin-modified thiol-ene microfluidic device for the solid-phase extraction of sugars and glycoproteins* (Undergraduate research project). University College Dublin, School of Biomolecular and Biomedical Science, 2025)

Methyl a- D -glucopyranoside = 99 97-30-3. (o. D.). https://www.sigmaaldrich.com/DK/en/product/sigma/m9376

Methyl a- D -mannopyranoside = 99.0 HPLC 617-04-9. (o. D.). https://www.sigmaaldrich.com/DK/en/product/sigma/m6882

Müller, C., Despras, G. & Lindhorst, T. K. (2016). Organizing multivalency in carbohydrate recognition. *Chemical Society Reviews*, *45*(11), 3275–3302. https://doi.org/10.1039/c6cs00165c

Nonis, S. G., Haywood, J., Schmidberger, J. W., Mackie, E. R. R., Da Costa, T. P. S., Bond, C. S. & Mylne, J. S. (2021). Structural and biochemical analyses of concanavalin A circular permutation by jack bean asparaginyl endopeptidase. *The Plant Cell*, *33*(8), 2794–2811. https://doi.org/10.1093/plcell/koab130

O'Connor, B. F., Monaghan, D. & Cawley, J. (2016). Lectin Affinity Chromatography (LAC). *Methods in Molecular Biology*, 411–420. https://doi.org/10.1007/978-1-4939-6412-3_23

Ocaña-González, J. A., Fernández-Torres, R., Bello-López, M. Á. & Ramos-Payán, M. (2015). New developments in microextraction techniques in bioanalysis. A review. *Analytica Chimica Acta*, *905*, 8–23. https://doi.org/10.1016/j.aca.2015.10.041

Pagaduan, J. V., Sahore, V. & Woolley, A. T. (2015). Applications of microfluidics and microchip electrophoresis for potential clinical biomarker analysis. *Analytical And Bioanalytical Chemistry*, *407*(23), 6911–6922. https://doi.org/10.1007/s00216-015-8622-5

Pflumm, M. N., Wang, J. L. & Edelman, G. M. (1971). Conformational changes in Concanavalin a. *Journal Of Biological Chemistry*, *246*(13), 4369–4370. https://doi.org/10.1016/s0021-9258(18)62095-2

Reddy, V. A., Johnson, R. S., Biemann, K., Williams, R. S., Ziegler, F. D., Trimble, R. B., & Maley, F. (1988). Characterization of the glycosylation sites in yeast external invertase. I. N-linked oligosaccharide content of the individual sequons. *The Journal of biological chemistry*, *263*(15), 6978–6985.

Reis, C. A., Osorio, H., Silva, L., Gomes, C. & David, L. (2010). Alterations in glycosylation as biomarkers for cancer detection. *Journal Of Clinical Pathology*, *63*(4), 322–329. https://doi.org/10.1136/jcp.2009.071035

Sainz-Polo, M., Ramírez-Escudero, M., Lafraya, A., González, B., Marín-Navarro, J., Polaina, J. & Sanz-Aparicio, J. (2013). Three-dimensional Structure of Saccharomyces Invertase. *Journal Of Biological Chemistry*, *288*(14), 9755–9766. https://doi.org/10.1074/jbc.m112.446435

Saleemuddin, M. & Husain, Q. (1991). Concanavalin A: A useful ligand for glycoenzyme immobilization—A review. *Enzyme And Microbial Technology*, *13*(4), 290–295. https://doi.org/10.1016/0141-0229(91)90146-2

Saleemuddin, M. (1999). Bioaffinity Based Immobilization of Enzymes. *Advances in Biochemical Engineering, Biotechnology*, 203–226. https://doi.org/10.1007/3-540-49811-7_6

Schmitt-Kopplin, P. & Fekete, A. (2016). The CE-Way of Thinking: "All Is Relative!". *Methods in Molecular Biology*, 3–19. https://doi.org/10.1007/978-1-4939-6403-1_1

Selzer, S. M., Vico, R. V. & Ferreyra, N. F. (2022). Immobilization of Concanavalin A on iron oxide magnetic nanoparticles. Effect of Bovine Serum Albumin in the recognition interactions of the lectin. *Surfaces And Interfaces*, *30*, 101908. https://doi.org/10.1016/j.surfin.2022.101908

Shang, Y., Zeng, Y. & Zeng, Y. (2016). Integrated Microfluidic Lectin Barcode Platform for High-Performance Focused Glycomic Profiling. *Scientific Reports*, *6*(1). https://doi.org/10.1038/srep20297

Sharon, N. (2004). History of lectins: from hemagglutinins to biological recognition molecules. *Glycobiology*, *14*(11), 53R-62R. https://doi.org/10.1093/glycob/cwh122

Shoham, M., Kalb, A. J. & Pecht, I. (1973). Specificity of metal ion interaction with concanavalin A. *Biochemistry*, *12*(10), 1914–1917. https://doi.org/10.1021/bi00734a012

Silsirivanit, A. (2019). Glycosylation markers in cancer. Advances in Clinical Chemistry, 189–213. https://doi.org/10.1016/bs.acc.2018.12.005

Sigma-aldrich. (n.d.). *Invertase from baker's yeast (S. cerevisiae), Catalog No. I4504 [Product information]*. Retrieved June 23, 2025, from https://www.sigmaaldrich.com/deepweb/assets/sigmaaldrich/product/documents/895/922/i4504pis.pdf

Smith, E. A., Thomas, W. D., Kiessling, L. L. & Corn, R. M. (2003). Surface Plasmon Resonance Imaging Studies of Protein-Carbohydrate Interactions. *Journal Of The American Chemical Society*, *125*(20), 6140–6148. https://doi.org/10.1021/ja034165u

Sønderby, C. (2018). *Development of a thiol-ene microfluidic device for on-chip reversed phase solid phase extraction of proteins and peptides with subsequent LC-MS analysis* (Master's thesis). Department of Pharmacy, School of Pharmaceutical Sciences, Faculty of Health and Medical Sciences, University of Copenhagen.

Sumner, J. B. & Howell, S. F. (1936). Identification of Hemagglutinin of Jack Bean with Concanavalin A. *Journal Of Bacteriology*, *32*(2), 227–237. https://doi.org/10.1128/jb.32.2.227-237.1936

Surya, P. H., Deepti, M. & Elyas, K. K. (2020). Plant Lectins: Sugar-Binding Properties and Biotechnological Applications. In *Springer eBooks* (S. 401–439). https://doi.org/10.1007/978-981-15-5136-9_17

Tanaka, N., Kobayashi, H., Ishizuka, N., Minakuchi, H., Nakanishi, K., Hosoya, K. & Ikegami, T. (2002). Monolithic silica columns for high-efficiency chromatographic separations. *Journal Of Chromatography A*, *965*(1–2), 35–49. https://doi.org/10.1016/s0021-9673(01)01582-5

Töpfer-Petersen, E., Romero, A., Varela, P. F., Ekhlasi-Hundrieser, M., Dostàlovà, Z., Sanz, L. & Calvete, J. J. (2009). Spermadhesins: A new protein family. Facts, hypotheses and perspectives. *Andrologia*, *30*(4–5), 217–224. https://doi.org/10.1111/j.1439-0272.1998.tb01163.x

Tousi, F., Hancock, W. S. & Hincapie, M. (2010). Technologies and strategies for glycoproteomics and glycomics and their application to clinical biomarker research. *Analytical Methods*, *3*(1), 20–32. https://doi.org/10.1039/c0ay00413h

Tran, N. T. & Taverna, M. (2016). Capillary Electrophoresis of Proteins and Peptides. In *Methods in molecular biology*. https://doi.org/10.1007/978-1-4939-4014-1

Van Damme, E. J. M. (2021). 35 years in plant lectin research: a journey from basic science to applications in agriculture and medicine. *Glycoconjugate Journal*, *39*(1), 83–97. https://doi.org/10.1007/s10719-021-10015-x

Xu, X., Peng, Q., Jiang, X., Tan, S., Yang, W., Han, Y., Oyang, L., Lin, J., Shen, M., Wang, J., Li, H., Xia, L., Peng, M., Wu, N., Tang, Y., Wang, H., Liao, Q. & Zhou, Y. (2024b). Altered glycosylation in cancer: molecular functions and therapeutic potential. *Cancer Communications*, *44*(11), 1316–1336. https://doi.org/10.1002/cac2.12610

Yang, Z. & Hancock, W. S. (2004). Approach to the comprehensive analysis of glycoproteins isolated from human serum using a multi-lectin affinity column. *Journal Of Chromatography A*, *1053*(1–2), 79–88. https://doi.org/10.1016/j.chroma.2004.08.150

Zeng, C. and Biemann, K. (1999), Determination of *N*-linked glycosylation of yeast external invertase by matrix-assisted laser desorption/ionization time-of-flight mass spectrometry †. J. *Mass Spectrom., 34: 311-329*. https://doi.org/10.1002/(SICI)1096-9888(199904)34:4<311::AID-JMS773>3.0.CO;2-F

Appendix

Appendix A:

From McLoughlin, A. (n.d.). *Development of a lectin-modified thiol-ene microfluidic device for the solid-phase extraction of sugars and glycoproteins* (Undergraduate research project). University College Dublin, School of Biomolecular and Biomedical Science.

Invertase was injected onto the chip in a stochiometric excess in 20 mM pH 5 citrate buffer, 2 mM metal ions. The incubation time was set to 1 hour, with a subsequent 60 min wash to remove non-bound invertase. Through competitive elution with a high concentrated MaM solution, the remaining bound invertase was eluted off the chip and collected in Eppendorf tubes. For the invertase assay, sucrose solutions were added to the fractions and incubated at 50°C and shaken at 350 rpm. To stop the hydrolysis the temperature was raised to 95°C. The amount of glucose (product of sucrose hydrolysis) was measured in the two wash fractions (fractions 1 and 2) and elute fractions (fractions 3 and 4) with CE-UV. As can be seen in Figure 13, glucose can only be detected in the elute fractions, indicating that the invertase proteins that were eluted off were catalytically active.

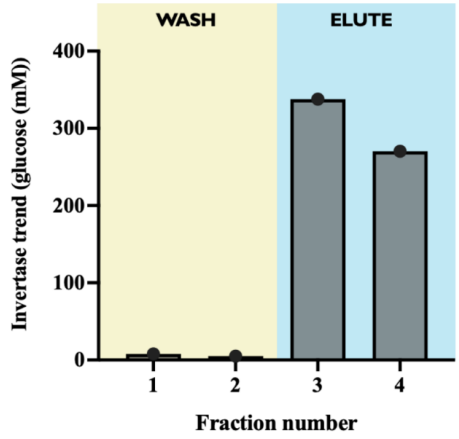

Figure 13: Invertase Assay

Appendix B:

Table 2: Optimized flow protocol for both SCC and LCC

Step	Buffer	Flow rate [µL/min]	Time [min]	Volume [µL]	Colum Volume	
					SCC	LCC
1 – Wash off non-Bound Lectin	20 mM Tris 0.5 M NaCl, 1mM $CaCl_2$, 1mM $MnCl_2$, pH 7.5	10 µL/min	10 LCC: 20	100 LCC: 200	100	~28
2 – Invertase Loading	Invertase in 20 mM Tris 0.5 M NaCl, 1mM $CaCl_2$, 1mM $MnCl_2$, pH 7.5	2 µL/min	30	60	60	~8
		Stop	30			
3 – Pre elution wash	MQ water, 1mM $CaCl_2$, 1mM $MnCl_2$	10 µL/min	10 LCC: 20	100 LCC: 200	100	~28
4 – Competitive Elution	1 M MαM in MQ water, 1mM $CaCl_2$, 1mM $MnCl_2$	Change Outlet tubing	7.5 7.5 7.5	45	45	~6
5 – Wash	20 mM Tris 0.5 M NaCl, 1mM $CaCl_2$,	10 µL/min	10 LCC: 20	100 LCC: 200	100	~28

	1mM $MnCl_2$, pH 7.5					
6 – Regeneration	20 mM Tris 0.5 M NaCl, 1mM $CaCl_2$, 1mM $MnCl_2$, pH 5.2	10 µL/min	10 LCC: 20	100 LCC: 200	100	~28
7 – Re-equilibration	20 mM Tris 0.5 M NaCl, 1mM $CaCl_2$, 1mM $MnCl_2$, pH 7.5, 2% Glucose	10 µL/min	10 LCC: 20	100 LCC: 200	100	~28

Appendix C:

Table 3: Amount of chip experiments and failure percentage.

Number of SCC exp.	24	SCC failure	37.50 %
Number of SCC Failures	9		
Number of LCC exp.	12	LCC failure	16.67 %
Number of LCC Failures	2		
Total number of tested Chips	36	Total Chip Failure	30.56 %

Appendix D:

Table 4: Formulars for calculations

Cross sectional Area	$A = w * h$	
Empty channel		
Flow Resistance without monolith	$R_{w.o.m} = \frac{12\eta L}{wh^3\left(1 - 0.63 \cdot \frac{h}{w}\right)}$	
Pressure Drop (Q = 2 µL/min or 10 µL/min) w.o. monolith	$\Delta P = R * Q$	
Hydraulic diameter	$D_h = \frac{2wh}{w + h}$	
Reynolds number	$Re = \frac{\rho\, u\, D_h}{\eta}$	
Monolith-filled channel		
Hydraulic permeability	$K = \frac{d_p^2 * e^3}{180 * (1 - e)^2}$	d_p = particle diameter, 1.4 nm e = 0.4 = Void volume with a 60% packing density
Darcys flow resistance	$R_m = \frac{\eta L}{K * A}$	
Superficial velocity	$v_s = \frac{Q}{A}$	
Interstitial velocity	$v_i = \frac{v_s}{e}$	
Residence time	$t_{res} = \frac{L}{v_i}$	
Reynolds number	$Re_m = \frac{\rho\, v_s\, d_p}{\eta}$	

Péclet number	$Pe_m = \frac{v_s\, d_p}{D}$	D = diffusion coefficient
Diffusion length between beads	$x = d_p * e^{\frac{1}{3}}$	
Diffusion time	$t_D = \frac{x^2}{2D}$	
Total surface area	$A_{tot} = N * A_{bead}$	N = Number of beads A_{bead} = Surface area of one bead
Coverage	$Cov = \frac{n * M}{A_{tot}}$	

Appendix E:

Python Script for calculations

```
import pandas as pd
import numpy as np

# ============================
# Define constants (editable)
# ============================
channel_length_mm = 10            # Channel length in mm (e.g., LCC 73)
channel_width_um = 500            # Channel width in micrometers (e.g., LCC 500)
channel_height_um = 300           # Channel height in micrometers (e.g., LCC 175)
viscosity_Pa_s = 0.001            # Dynamic viscosity of fluid (Pa·s), e.g. water
Q_2ul = 2e-9 / 60                 # Volumetric flow rate 2 µL/min converted to m³/s
Q_10ul = 10e-9 / 60               # Volumetric flow rate 10 µL/min converted to m³/s
packing_density = 0.6             # Porosity (ε), typical value for packed bed
Dp = 1.4e-6                       # Bead diameter in meters (1.4 µm)
D = 3.35645532292877e-11          # Diffusion coefficient for Invertase in m²/s
rho = 1000                        # Fluid density in kg/m³ (water)

# ============================
# Convert channel dimensions to SI units
# ============================
channel_width_m = channel_width_um * 1e-6       # Convert width from µm to m
channel_height_m = channel_height_um * 1e-6     # Convert height from µm to m
channel_length_m = channel_length_mm * 1e-3     # Convert length from mm to m

# Calculate cross-sectional area in m² and mm²
cross_section_m2 = channel_width_m * channel_height_m
cross_section_mm2 = cross_section_m2 * 1e6      # Convert m² to mm²

# Calculate channel volume in m³ and µL
volume_m3 = cross_section_m2 * channel_length_m
volume_ul = volume_m3 * 1e9                     # Convert m³ to µL

# ============================
# Empty channel (no monolith) flow resistance and pressure drop
# ============================
# Aspect ratio for rectangular channel (height/width)
aspect_ratio = channel_height_m / channel_width_m

# Correction factor for rectangular channel flow
correction = 1 - 0.63 * aspect_ratio

# Hydraulic resistance (Pa·s/m³)
R_empty = (12 * viscosity_Pa_s * channel_length_m) / (channel_width_m * channel_height_m**3 * correction)

# Pressure drop at 2 µL/min (Pa and mbar)
DP_2ul_empty = R_empty * Q_2ul
DP_2ul_empty_mbar = DP_2ul_empty / 100  # Convert Pa to mbar

# Pressure drop at 10 µL/min (Pa and mbar)
```

```
DP_10ul_empty = R_empty * Q_10ul
DP_10ul_empty_mbar = DP_10ul_empty / 100  # Convert Pa to mbar

# ============================
# Reynolds number for empty channel flow
# ============================
# Hydraulic diameter (m) for rectangular channel
hydraulic_diameter_m = 2 * (channel_height_m * channel_width_m) / (channel_height_m + channel_width_m)

# Average velocity for 2 µL/min and 10 µL/min flow rates (m/s)
u_avg_velocity_2ul = Q_2ul / cross_section_m2
u_avg_velocity_10ul = Q_10ul / cross_section_m2

# Reynolds number for 2 µL/min and 10 µL/min flow
Re_2ul_empty = (rho * u_avg_velocity_2ul * hydraulic_diameter_m) / viscosity_Pa_s
Re_10ul_empty = (rho * u_avg_velocity_10ul * hydraulic_diameter_m) / viscosity_Pa_s

# ============================
# Packed bed (monolith) calculations
# ============================
# Total porosity (assumed)
epsilon_tot = packing_density  # Typically ~0.6 for packed bed

# Kozeny–Carman permeability constant denominator
kc_correction = 180 * (1 - epsilon_tot)**2

# Permeability K (m²)
K = (Dp**2 * epsilon_tot**3) / kc_correction

# Monolith hydraulic resistance (Pa·s/m³)
R_mono = (viscosity_Pa_s * channel_length_m) / (K * cross_section_m2)

# Pressure drop at 2 µL/min and 10 µL/min through monolith (Pa, mbar, psi)
DP_2ul_mono = R_mono * Q_2ul
DP_2ul_mono_mbar = DP_2ul_mono * 1e-2
DP_2ul_mono_psi = DP_2ul_mono / 6894.76

DP_10ul_mono = R_mono * Q_10ul
DP_10ul_mono_mbar = DP_10ul_mono * 1e-2
DP_10ul_mono_psi = DP_10ul_mono / 6894.76

# ============================
# Velocity calculations
# ============================
# Superficial velocities (m/s)
v_superficial_2ul = Q_2ul / cross_section_m2
v_superficial_10ul = Q_10ul / cross_section_m2

# Interstitial velocities (m/s)
v_interstitial_2ul = v_superficial_2ul / epsilon_tot
v_interstitial_10ul = v_superficial_10ul / epsilon_tot

# Interstitial velocities in cm/min for convenience
v_interstitial_2ul_cm_min = v_interstitial_2ul * 60 * 100
v_interstitial_10ul_cm_min = v_interstitial_10ul * 60 * 100

# Residence time in seconds inside the monolith (length / velocity)
residence_time_2ul = channel_length_m / v_interstitial_2ul
residence_time_10ul = channel_length_m / v_interstitial_10ul

# ============================
# Dimensionless numbers (Reynolds and Peclet)
# ============================

# Reynolds number for flow inside packed bed
Re_2ul = (rho * v_superficial_2ul * Dp) / viscosity_Pa_s
Re_10ul = (rho * v_superficial_10ul * Dp) / viscosity_Pa_s
```

```
# Peclet number (advection/diffusion ratio)
Pe_2ul = (v_superficial_2ul * Dp) / D
Pe_10ul = (v_superficial_10ul * Dp) / D

# Shear stress on channel wall (Pa)
shear_stress = viscosity_Pa_s * v_superficial_2ul / channel_height_m

# ============================
# Diffusion calculations
# ============================
# Diffusion distance within porous media (m)
diffusion_distance = Dp * epsilon_tot**(1/3)

# Diffusion time (s)
diffusion_time = diffusion_distance**2 / (2 * D)

# Ratios of diffusion time to residence time
ratio_2ul = diffusion_time / residence_time_2ul
ratio_10ul = diffusion_time / residence_time_10ul

# ============================
# Bead surface area and ConA coverage calculations
# ============================
# Bead radius (m)
r_bead = Dp / 2

# Surface area of one bead (m²)
A_bead = 4 * np.pi * r_bead**2

# Volume of one bead (m³)
V_bead = (4/3) * np.pi * r_bead**3

# Packed bed volume (m³)
packed_bed_volume = volume_m3 * packing_density

# Number of beads in packed bed
N_beads = packed_bed_volume / V_bead

# Total surface area of beads (m² and cm²)
total_surface_area = A_bead * N_beads
total_surface_area_cm2 = total_surface_area * 1e4  # Convert m² to cm²

# Area occupied by one ConA molecule (m²)
diameter_conA = 7.7e-9
area_occupied_by_1_conA = diameter_conA**2

# Number of ConA molecules that could occupy total bead surface
mole_of_ConA = total_surface_area / area_occupied_by_1_conA

# ============================
# ConA concentration and amount calculations
# ============================
conc_conA_mg_per_ml = 10          # Concentration of ConA in mg/mL
ug_conA = 600                     # Total amount of ConA in µg
g_ConA = ug_conA / 1e6            # Convert µg to g
Mw_ConA = 106000                  # Molecular weight of ConA (g/mol)

# Total moles of ConA
tot_mol = g_ConA / Mw_ConA
tot_pmol = tot_mol * 1e12         # Convert mol to pmol

# Area occupied by all ConA molecules (cm²)
area_occupied_by_all_conA = tot_mol * area_occupied_by_1_conA * 1e4

# ============================
# Max and min surface coverage estimates
# ============================
# Max pmol of invertase interacting
```

```
pmol_of_Inv_max = 15
mol_of_Inv_max = pmol_of_Inv_max * 1e-12
g_ConA_max = mol_of_Inv_max * Mw_ConA
ng_ConA_max = g_ConA_max * 1e9

surface_coverage_max = ng_ConA_max / total_surface_area_cm2  # ng/cm²

# Min pmol of invertase interacting
pmol_of_Inv_min = 7.5
mol_of_Inv_min = pmol_of_Inv_min * 1e-12
g_ConA_min = mol_of_Inv_min * Mw_ConA
ng_ConA_min = g_ConA_min * 1e9

surface_coverage_min = ng_ConA_min / total_surface_area_cm2  # ng/cm²

# ============================
# Average spacing between molecules (m)
# ============================
concentration_per_volume = 1  # mol/m³ (example value)
average_spacing = (1 / concentration_per_volume)**(1/3)
```